RESEARCH

Structural Investigation and Optical Properties of Dysprosium (Dy^{3+}) Ions Doped Oxyfluoro Antimony Borate Glasses for Photonics Applications

Ch. Pravallika^1 · K. Swapna^1 · Ib Singh Deo^2 · Sk. Mahamuda^1 · M. Venkateswarulu^1 · A. S. Rao^3 · Vijaya Prakash G.^{2}

Abstract

Dysprosium oxide-doped glasses with a composition of $60B_2O_3$-$10Sb_2O_3$-$10Al_2O_3$-$10NaF$-$(10-x)$ LiF-xDy_2O_3 (x = 0.1, 0.5, 1.0, 1.5, 2.0, 2.5 mol%) were prepared using a conventional melt-quenching technique. The glasses were characterized through various analytical investigations, including X-ray diffraction (XRD), Fourier transform infrared (FTIR) spectroscopy, refractive index, density, optical absorption, excitation, photoluminescence (PL) studies, decay measurements and radiation shielding parameters. The XRD and FT-IR confirms the glassy nature and functional groups present in the titled glass. The absorption spectra were used to determine the oscillator strength of the Dy^{3+} absorption transitions as well as the bond created with the O^{-2} ion in the titled glass network. The degree of the suitability of developed glasses for lasing applications was demonstrated by radiative parameters determined using Judd–Ofelt theory. In the prepared glass samples, the optical bandgap measurements indicate the presence of non-bridging oxygen (NBOs), localization of charges and donor centers in the titled glasses. Due to the de-excitation of $^4F_{9/2}$ to the corresponding $^6H_{15/2}$, $^6H_{13/2}$ and $^6H_{11/2}$ states, the PL emission spectrum shows two main strong emissions at blue(480nm), yellow (575nm) and one less emission at red (663nm). The CIE coordinates determined using PL emission spectra reveal the coordinates that are falling within the white light region. Various shielding parameters such as mass attenuation coefficient, mean free path, effective atomic number were estimated to understand the radiative shielding nature of the titled glasses. Within the addition of Dy_2O_3, it was found that the shielding parameters values of the titled glass samples are increasing. The Mass Attenuation Coefficient, Half Value Layer and Mean Free Path of the as prepared glasses has been compared with different types of concretes to understand the shielding effectiveness of prepared glass.

Keywords Dy^{3+} ions · Absorption · J-O parameters · PL Studies · Radiation shielding parameters

Introduction

The rare-earth (RE) doped materials have gained considerable attention owing to their potential applications in many fields, like medicine, optoelectronics, and telecommunication (optical fibers, lasers, and amplifiers) because RE ions exhibit emission transitions in 4f-4f or 4f-5d, additionally their unique electronic configuration from the ultraviolet region to the infrared region makes them to act as an excellent activator to emit sharp luminescence [1–3]. In particular, glasses doped with RE ions have gained significant attention for the development of Solid-State Lighting devices (SSL). The SSL technology is used in many lighting applications because of its advantages like durability, energy saving and eco-friendly [4]. In SSL, white light-emitting diodes (wLEDs) are an interesting possible substitute for fluorescent lamps because of their advantageous properties such as transparency, thermal stability, and low cost. Currently, blue or near-ultraviolet LED chips are used to excite phosphors (YAG: Ce^{3+}, for example) in epoxy resin to provide white light. To achieve great brightness, however, the output power of the LEDs must be raised, which raises the chip's temperature. The resin can break down as a result of the temperature rise, which would lower the light's quality and intensity. Since they may be made in the form of a lens,

✉ K. Swapna
  kswapna80@gmail.com

1 Department of Physics, Koneru Lakshmaiah Education Foundation, Vaddeswaram, Andhra Pradesh, India

2 Nanophotonics Lab, Department of Physics, Indian Institute of Technology, Delhi, New Delhi 110016, India

3 Department of Applied Physics, Delhi Technological University, Bawana Road, New Delhi 110042, India

luminescent materials doped with trivalent RE ions can be utilized to replace the phosphor particles to promote direct encapsulation of the LED chip [5].

On the other hand, the RE ions are using to replace the concretes [6] which are opaque and unclear to visible light, as alternative gamma ray shielding materials for various uses in high energy physics applications and nuclear waste management. The gamma rays which may lead to increase the risks for cancer, damage to human cells, and environmental effects. Therefore, the use of reliable shields is fundamental. Radiation shields are the most widely used materials because of their high density, good structural properties, and cost efficiency. Although lead is a very efficient shielding material but it is highly toxic and harmful to the environment; therefore, the present research is focused on non-toxic alternatives [7]. Numerous studies have been reported to replace the lead-based glass with different types of glass matrices like borates [8], silicates [9], phosphates [10], tellurites [11], etc., borate glasses are well-suited application for the prepared glasses [12–14].Boric acid (B_2O_3) is one of the excellent glass former in oxide materials because it has a high glass-forming trend and exhibits unique advantages, like minimum dielectric constant, ease of formation, low melting point, low cost, high RE ion solubility, and good transparency. Borate glasses are suitable for a variety of applications in fiberglass as they tend to reduce thermal expansion and resist thermal shock at high temperature. However, the main drawback of borate glasses is that, they possess a phonon energy of approximately 1300 cm^{-1}, which is relatively quite high because the presence of lightweight which possess relatively high phonon energy. Such high phonon energies increase nonradiative loss through the multiphonon relaxation process. Heavy metal oxides like bismuth, tellurite, tungsten, and antimony have attracted attention because of their relatively low phonon energies, high polarizabilities, and high refractive indices [15]. In addition to the this, alkali fluorides such as NaF and LiF in the glass minimizes the non-radiative energy loss and decreases the phonon energy. Such alkali fluorides also help to remove the -OH groups present in the borate glasses. In addition, Aluminum Oxide (Al_2O_3), as a glass modifier, provides mechanical strength to glass and improves its optical response. The thermal and chemical properties also enhanced the emission properties of the prepared glass samples [16]. By adding the Al_2O_3 to a borate glass matrix it can form the AlO_4 and AlO_6 units [17].

Among lanthanides, Dysprosium ions (Dy^{3+}), is a promising ion for white-light devices and visible-laser applications. It has distinct emission bands between the visible and near-infrared regions, which lend themselves to a variety of interesting optical properties. Due to electronic transitions at $^4F_{9/2} \rightarrow {}^6H_{15/2}$, $^4F_{9/2} \rightarrow {}^6H_{13/2}$, and $^4F_{9/2} \rightarrow {}^6H_{11/2}$, Dy^{3+} ions primarily exhibit two strong emission bands, which are pure magnetic dipole transition at blue (470–500 nm) and pure electric dipole transition at yellow (570–600 nm) regions, as well as one weak red emission band (660–700 nm). Among these, the hypersensitive transition $^4F_{9/2} \rightarrow {}^6H_{13/2}$ is strongly affected by the environment. Emission of white light at a regulated yellow to blue (Y/B) ratio can be achieved by adjusting the concentration of dysprosium ions in a host matrix and adjusting excitation wavelength. The Y/B ratio also provides information on the Dy^{3+} -O^{2-} ion environment in the nearby regions of the dysprosium ions, such as the degree of covalence. Both visible and near-infrared solids state lasers can be created through glasses doped with Dy^{3+} ions [18, 19].

In the present work, we synthesized the Dy^{3+} ions activated $60B_2O_3$-$10Sb_2O_3$-$10Al_2O_3$-$10NaF$-(10-x) LiF-xR.E (OFSbB) glass samples were synthesized and characterized them by using XRD, FT-IR and optical properties such as absorption, luminescence spectra and decay time measurements. Evaluation of Judd-Oflet (J-O) intensity parameters and their trends, as well as physical parameters, were investigated with respect to Dy^{3+} concentration. The optical bandgap energy was estimated using Tauc's plot for the indirect and direct transitions from the absorption data. Under excitation at 351 nm, the yellow-blue (Y/B) intensity ratio results in the application of white-light-emitting devices. The PSD software was used to investigate OFSbBDy glasses gamma-ray shielding parameters, including the Effective Atomic Number, Linear Attenuation Coefficient, Half Value Layer, Tenth Value Layer, Mean Free Path, Mass Attenuation Coefficient, and Exposure Buildup Factor.

Experimental Approach

Synthesis

The Melt-quenching method was used to synthesize the Dy^{3+} ions-doped glass with a $60B_2O_3$-$10Sb_2O_3$-$10Al_2O_3$-$10NaF$-(10-x) LiF-xDy_2O_3 composition (where, x=0.1, 0.5, 1.0, 1.5, 2.0, 2.5 mol %). The prepared glasses are referred to as OFSbBDy0.1, OFSbBDy0.5, OFSbBDy1.0, OFSbBDy1.5, OFSbBDy2.0, and OFSbBDy2.5, depending on the Dy-ion concentration from 0.1 to 2.5mol% respectively. All the chemicals were weighed using an electrical weighing balance with an appropriate molecular weight. After weighing, the chemical composition was ground into a fine powder using an agate mortar and pestle. The batch materials, which were placed in silica crucibles and heated for ten minutes at 1200 °C in an electric furnace, had a stoichiometric composition of approximately 8 g. The melt was kept homogeneous by being stirred every three minutes. To eliminate the internal thermal stress caused by the quenching process, the melt was quenched in a brass mold and plates that had been preheated and then annealed for two hours at 500 °C. The prepared glasses had a 2 mm thickness and were transparent.

Sample Characterization

Using Cu K ($\lambda = 1.5405$Å) radiation, an XRD analysis of the prepared glasses amorphous nature was performed on PANalytical EMPRYREAN diffractometer. The densities and refractive index of the glass samples were measured using Archimedes rule and Brewster's angle method respectively. FT-IR spectra of the glass samples were recorded using a JASCO FT/IR- 4700 spectrometer. A JASCO V-670 UV–vis-NIR spectrometer was utilized for the recording of the absorption spectra. Using a JASCO FP-8300 spectrofluorometer, excitation, PL spectra and PL decay curves of the as prepared glass samples were recorded at room temperature. The characteristics of photon shielding for the OFSbBDy glasses were computed using the PSD/Phy-X software [20].

Results and Discussion

Structural Analysis

X-ray Diffraction

Figure 1 shows the patterns of X-Ray Diffraction at the different concentrations of Dy^{3+} ions-activated OFSbB glass samples recorded in the 2θ range of 20–80° on a PANalytical EMPYREAN diffractometer with Cu Kα ($\lambda = 1.5405$Å) radiation. In general, non-crystalline materials do not exhibit sharp peaks because of the nonperiodic arrangement of atoms in these solids, which does not satisfy the diffraction condition [21]. The prepared glass samples exhibited a broad hump at approximately 27°, indicating the presence of the BO_3 group [5].

Fourier Transform Infrared Spectroscopy

FT-IR plays an important role in determining the structural properties of the as prepared glass samples. Figure 2 represents the FT-IR spectra of Dy^{3+} ions-doped and un-doped OFSbB glass samples, which were recorded in the wavelength range from 450 to 3500 cm^{-1}. The BO_3 group is present, as an evidenced by the peak at $512cm^{-1}$. The bending vibrations of the BO – O– BO_4 bonds is attributed due to the peak at $688cm^{-1}$. The peak at 891 cm-1 corresponds to the stretching vibrations of the tetrahedral BO_4^{-1} units. The peak at 1047 cm^{-1} indicates the pentaborane group. The peaks at 1209 cm^{-1} represent the B-O-B bending vibrations in the tetrahedra corresponding to boron-tetrahedral units. The peak at 1335 cm^{-1} represents the stretch vibration between Boron-Oxygen bonds of the BO_3 unit, which also results about the link between oxygen and different connecting diverse groups like orthoborate, metaborate and pyroborate. The peak at 2345 cm^{-1} indicates the presence of hydrogen bonds in the prepared glasses. The peak at 3057 cm^{-1} indicates the presence of the OH group [22–25].

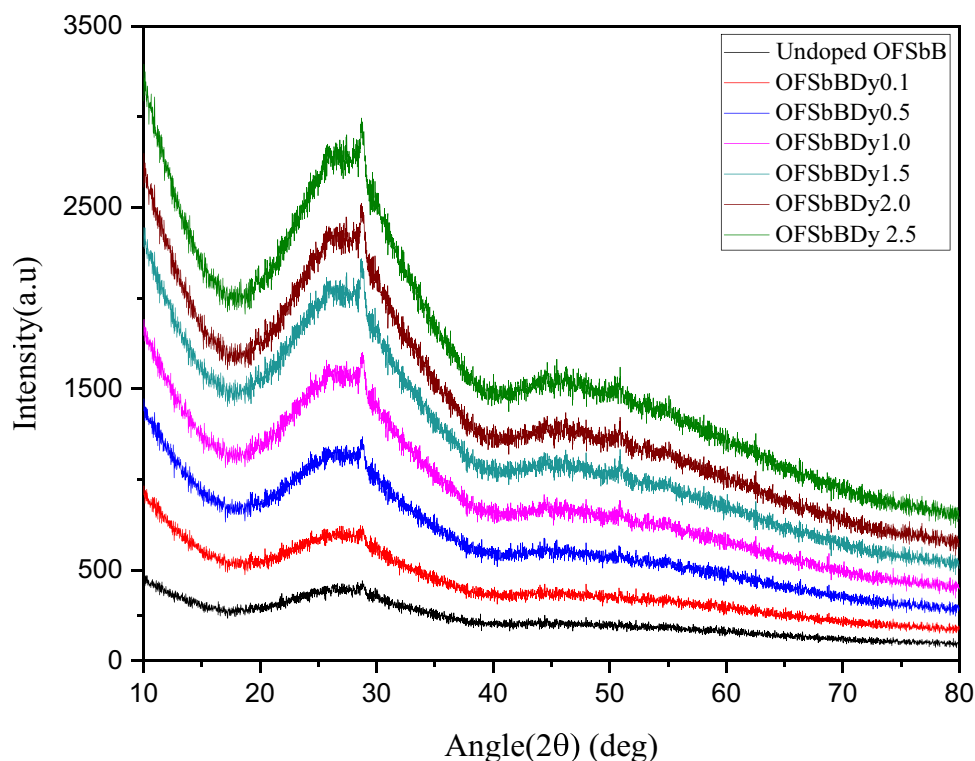**Fig. 1** The X-Ray Diffraction patterns of the undoped and doped OFSbBDy glass samples
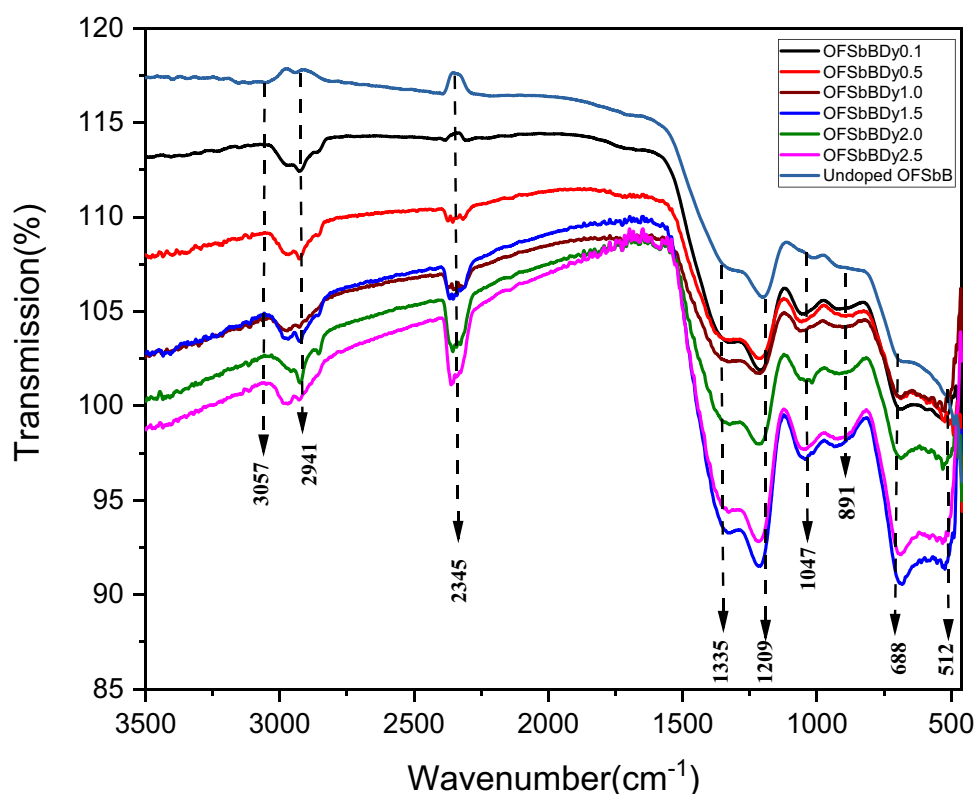
Fig. 2 The Fourier transform infrared (FTIR) spectra of the Dy^{3+} ions doped into the OFSbB glass samples

Physical Parameters

Table 1 describes Physical parameters of Dy^{3+} ions doped OFSbB glasses like refractive index(n), density, RE ion concentration(N), average molecular weight(M), polaron radius(r_p), inter-ionic distance(r_i), and field strength(F) of the prepared glasses. The OFSbB glasses density increased with an increase in Dy^{3+} ions concentration. The density increased because of the increase in the molar mass and modifications of the BO$_3$ triangles in to BO^{-4} tetrahedra. The density depends on the alkali type and alkali earth modifier, which occupy the interstitial positions in the glass network. The Li$^+$ ion connects with the glass former cations, that is with B^{3+} ions, and enhances ring-type structures and coordination numbers, which also leads to a increase in density because of the presence of Non-Bridging Oxygen (NBO) atoms

Table 1 Physical parameters of Dy^{3+} ions doped OFSbB glasses

Physical Parameters	OFSbBDy0.1	OFSbBDy0.5	OFSbBDy1.0	OFSbBDy1.5	OFSbBDy2.0	OFSbBDy2.5
Refractive index (n_d)	2.243	2.252	2.256	2.259	2.267	2.271
Density (g/cc)	2.916	2.936	2.962	2.988	3.014	3.04
Average molecular weight (g)	83.586	94.452	96.187	97.922	99.658	101.393
Dy^{3+} ion concentration ($\times 10^{22}$ ions/cm^3)	0.034	0.172	0.341	0.506	0.668	0.826
Mean atomic volume (g/cm^3/atom)	6.901	7.721	7.767	7.867	7.853	14.208
Dielectric constant (Ɛ)	5.031	5.071	5.089	5.103	5.139	5.157
Optical dielectric constant(P$\partial t/\partial p$)	4.031	4.071	4.089	4.103	4.139	4.157
Reflection losses (R)	0.146	0.148	0.148	0.149	0.150	0.150
Molar refraction R$_m$ (cm^{-3})	16.435	18.517	18.728	18.928	19.169	19.373
Polaron radius (Å)	5.816	3.413	2.720	2.385	2.175	2.026
Interionic distance (Å)	0.144	8.470	6.750	5.919	5.398	5.029
Molecular electronic polarizability ($\times 10^{-23}$ cm^3)	0.392	7.958	4.032	2.722	2.071	1.677
Field strength ($\times 10^{15}$ cm^2)	0.886	2.574	4.053	5.270	6.338	7.302

in dysprosium oxide. The refractive indices of the glasses increased with increasing Dy^{3+} ions concentration because the polarizability of oxide increase with rare earth ions and also related to the density. The prepared glasses result the low molar electronic polarizability value results the increase in the glass network stability because the molar polarizability connected to macro and micro, physical, chemical properties like UV absorption, chemical stability [14, 26].

Absorption Spectral Analysis

Figure 3 shows the absorption spectral data of the Dy^{3+} ions-doped OFSbB glasses, which were recorded at room temperature from the ultraviolet–visible to near-infrared region. The absorption spectra show twelve peaks that are arising due to f-f transition from the ground energy state $^6H_{15/2}$ to various higher energy states of the doped dysprosium ions. The twelve electronic transitions of the absorption bands from $^6H_{15/2}$ ground state are $^4M_{15/2}$, $^6P_{5/2}$, $^4I_{13/2}$, $^4G_{11/2}$, $^4I_{15/2}$, $^4F_{9/2}$, $^6F_{3/2}$, $^6F_{5/2}$, $^6F_{7/2}$, $^6F_{9/2}$, $^6F_{11/2}$, $^6H_{11/2}$ with the energies 350, 364, 387, 426, 451, 473, 683, 753, 802, 901, 1092, 1275 and 1684 nm respectively. All electronic transitions were identified according to a report available in literature [27]. The resultant band peak intensity exhibiting high energy in the UV region is weak because of less absorption, and the low-energy near-infrared region (NIR) exhibits a strong absorption titled host matrix. The Dy^{3+} ions electronic configuration is $4f^9$, which results in a ground state multiplet (^6H), a high-intensity band at 1275 nm in the near-infrared region, and free ions in the ultraviolet region because of the overlapping of different $^{2S+1}L_J$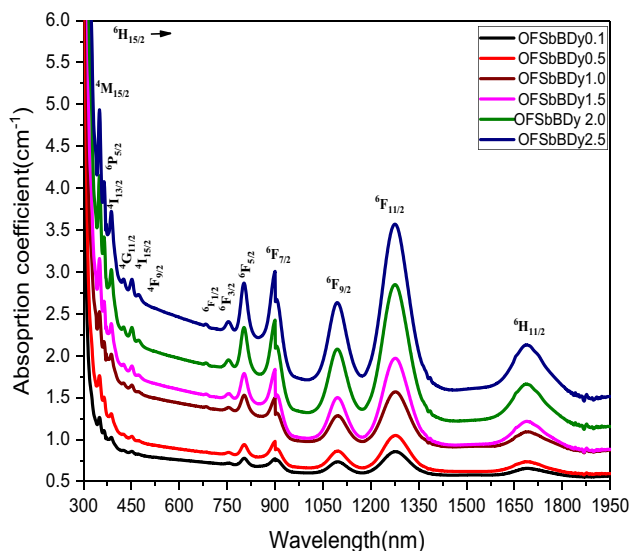 levels. The spectra exhibited high intensity because of the hypersensitive nature of the $^6H_{15/2} \rightarrow {}^6F_{11/2}$ electronic transition, and obeyed the selection rules $|\Delta S| = 0$, $|\Delta L| \leq 2$, and $|\Delta J| \leq 2$ [28]. The electronic transition between the ground state ($^6H_{15/2}$) and excited states (^6H, ^6F) exhibited sharp and intense bands, owing to their spin-allowed nature.

Nephelauxetic Effects and Bonding Parameters

From the optical absorption spectra, the bonding nature of Dy-O in the OFSbB glass was determined. The nephelauxetic ratio (β) and the bonding parameter (δ) studies were used to determine the Dysprosium ion ligand's bonding nature. The following equations are used to determine the Nephelauxetic ratio:

$$\beta = \frac{\vartheta_c}{\vartheta_a} \tag{1}$$

where, ϑ_c is the wavenumber (cm^{-1}) of a specific shift of the rare earth ions & ϑ_a stands the wavenumber (cm^{-1}) for the similar shift of an aqua ion. The δ is calculated by the following equation.

$$\delta = \frac{1 - \overline{\beta}}{\overline{\beta}} \tag{2}$$

Here, $\overline{\beta}$ is the average of β value. `based upon the environment of δ results either positive or negative which indicates the covalent or ionic nature if bonding. The bonding parameter of the prepared Dy^{3+} ions-doped OFSbB glass was negative, -0.936, -0.932, -0.930, -0.929, -0.924, and -0.923 for 0.1,0.5,1.0,1.5,2.0 and 2.5 mol% indicating ionic bonding. It indicates that when the concentration of RE ions increases, the ligand network surrounding the RE ions changes. The number of NBO's in the glass matrix, which are reason for the large changes in bonding parameter values, is also influenced by the doping concentration. The prepared glass samples, a decrease in ionicity corresponds to a reduction of bonding defects.

Optical Bandgap Analysis

Optical bandgap analysis was used to determine the bandgap between the conduction and valence bands in the oxide glasses. The nature of the glass structure and chemical bonding can be explored by analyzing the optical absorption spectral transitions [27, 29, 30]. By calculating the absorption coefficient α(ν), information about the induced transitions, such as direct and indirect allowed transitions, can be obtained. From the Davis and Mott theory, the following expression is used to evaluate the absorption coefficient [31].

Fig. 3 The absorption spectra Dy^{3+} ions doped OFSbB glass samples

$$\alpha h\nu = B\left(h\nu - E_g\right)^n \qquad (3)$$

where B is the band tailing parameter, E_g is the bandgap energy & n = 1/2 or 2, depends upon either indirect allowed transition or direct allowed transition, respectively. By using Tauc plot $((\alpha h\nu)^{1/n}$ vs. $h\nu)$ the E_g values of the OFSbBDy glasses were determined through extrapolating the linear portion of the curve. Figure 4 represents the Tauc plot for indirect (n = 1/2) and direct (n = 2) transitions of the prepared glasses.

Estimation of Oscillator Strengths and Judd–Ofelt Intensity Parameters

The oscillator strengths are determined using the J–O theory, which explains the strength of the absorption peaks of RE ions. This determines the integration of the area under the curve of each observed band. Using the equation given below, the experimental oscillator strength(f_{exp}) was calculated as follows:

$$f_{exp} = 4.318 \times 10^{-9} \int \varepsilon(\nu)d\nu \qquad (4)$$

Here, $\mathcal{E}(\nu)$, ν addresses the molar absorption of the peak(cm^{-1}), frequency of specific band.

Additionally, the following formula can be used to estimate the calculated oscillator strength(f_{cal}) during the primary and final state transitions [32, 33]:

$$f_{cal} = \frac{8\pi^2 mc}{3h} \frac{(n^2+2)^2}{9n} \frac{\nu}{(2J+1)} \sum_{\lambda=2,4,6} \Omega_\lambda \left(\psi J\|U^\lambda\|\psi'J'\right)^2 \qquad (5)$$
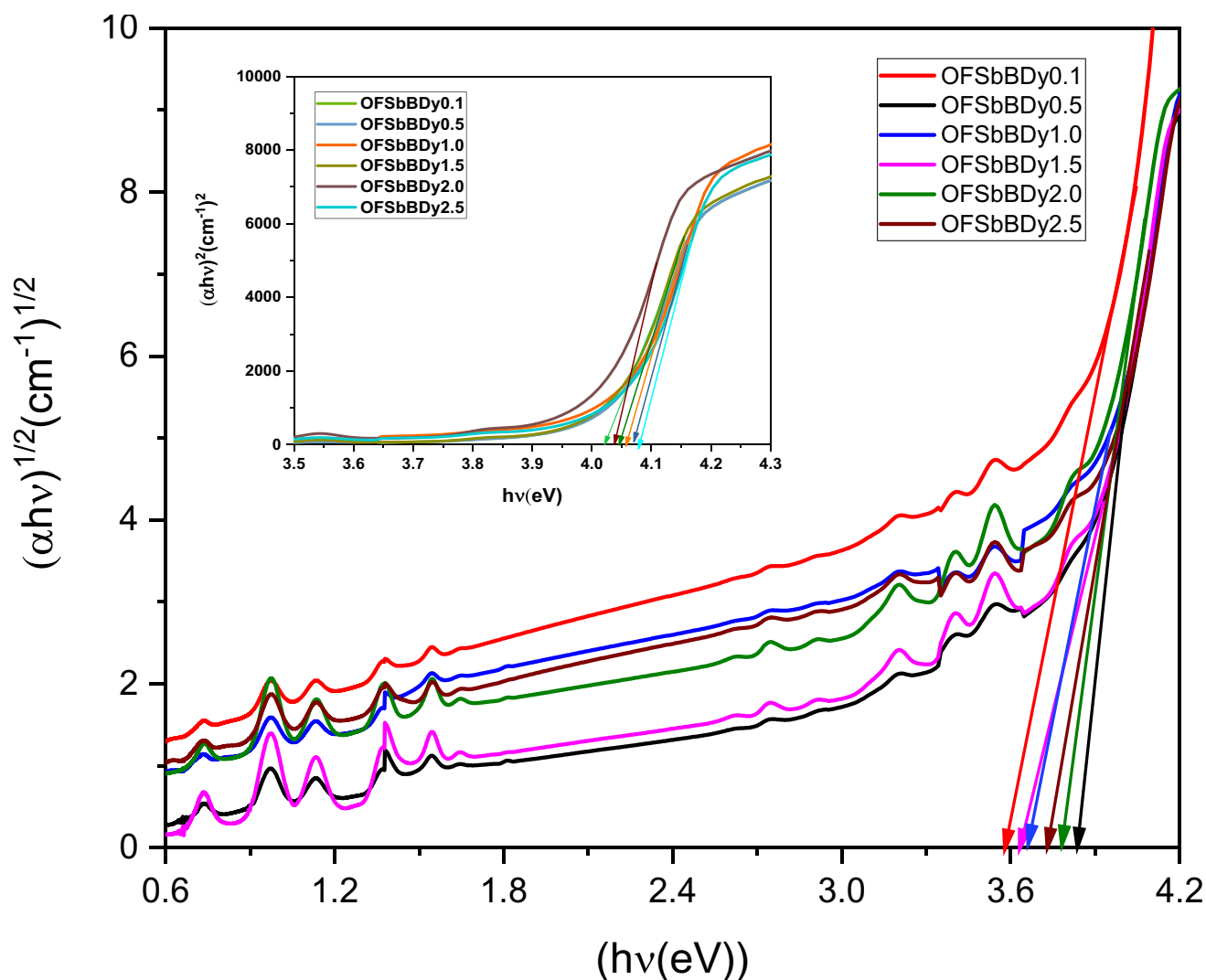

Fig. 4 The indirect band gap of Dy^{3+} ions doped OFSbB glass samples. The inset shows direct band gap of Dy^{3+} ions doped OFSbB glass samples

Table 2 The oscillator strength (f_{exp} and f_{cal} X 10^{-6}), rms deviation ($\delta_{rms} \times 10^{-6}$) of the OFSbBDy glasses for different absorption bands

Transition	OFSbBDy0.1		OFSbBDy0.5		OFSbBDy1.0		OFSbBDy1.5		OFSbBDy2.0		OFSbBDy2.5	
$^6H_{15/2} \rightarrow$	f_{exp}	f_{cal}	f_{exp}	f_{cal}	f_{exp}	f_{cal}	f_{exp}	f_{cal}	f_{exp}	f_{cal}	f_{exp}	f_{cal}
$^4M_{15/2}$	0.154	0.093	0.617	0.106	0.58	0.951	0.389	0.091	0.28	0.073	0.245	0.055
$^6P_{5/2}$	1.714	1.714	2.062	2.085	1.891	1.891	1.757	1.684	1.12	1.142	1.04	0.794
$^4I_{13/2}$	0.814	0.691	1.634	0.826	1.074	0.726	1.201	0.669	0.954	0.472	0.761	0.336
$^4G_{11/2}$	1.525	1.539	1.994	1.861	1.567	1.64	1.464	1.516	1.261	1.055	1.184	0.746
$^4I_{15/2}$	1.027	0.175	1.647	0.134	1.095	0.098	0.924	0.033	0.68	0.039	0.483	0.033
$^4F_{9/2}$	0.841	0.606	1.065	0.715	0.597	0.619	0.52	0.548	0.346	0.376	0.239	0.263
$^6F_{1/2}$	-	-	1.836	0	0.793	0	0.654	0	0.517	0	0.351	0
$^6F_{3/2}$	0.96	0.725	1.096	0.882	0.957	0.773	0.998	0.706	0.64	0.479	0.419	0.333
$^6F_{5/2}$	3.496	3.842	4.709	4.673	3.744	4.103	3.559	3.749	2.752	2.539	1.151	1.764
$^6F_{7/2}$	6.788	7.841	8.591	9.163	6.511	7.989	5.882	7.029	3.147	4.836	2.118	3.39
$^6F_{9/2}$	8.804	8.544	9.217	9.093	7.998	7.635	6.32	6.043	4.74	4.338	3.432	3.106
$^6F_{11/2}$	11.73	11.799	12.324	12.324	10.49	10.583	9.236	9.305	7.68	7.766	5.91	5.999
$^6H_{11/2}$	4.564	4.035	5.05	4.825	4.952	4.237	4.418	3.892	3.39	2.736	2.616	1.944
RMS(δ)	0.45		0.746		0.619		0.511		0.59		0.509	

The plank constant, electron mass, refractive index, and wavenumber (in cm^{-1}) are all represented here by h, m, n and ν respectively. The angular momentum from the ground start to the excited state is represented by J (J = L + S); the absorption band's Lorentz local field correction is $(n^2 + 2)^2/9n$; the host-dependent J-O intensity parameters and U^λ are the host-independent elements of the unit tensor square matrix. The following expression is used to evaluate the quality of fitting between the f_{exp} and f_{cal} data using root mean square deviation(δ_{rms}). The following expression is used to evaluate the quality of fitting between the f_{exp} and f_{cal} data using δ_{rms}.

$$\delta_{rms} = \sqrt{\frac{\sum \left(f_{exp} - f_{cal}\right)^2}{N}} \quad (6)$$

where N represents the level. Table 2 shows the f_{exp}, f_{cal} and δ_{rms} values of the as prepared glass samples. The three calculated J-O intensities $\Omega_\lambda(\lambda = 2,4,6)$ parameters are shown in Table 3. The parameters demonstrate nature of the local arrangement and bonding nature of the RE ions. From the Table 3, the evaluated Ω_λ values results the same trend ($\Omega_2 > \Omega_6 > \Omega_4$) for all the titled glasses. From Jorgensen and Reisfeld theory [34], the covalent valence of the metal–ligand bond and the asymmetry of the ion sites in the ligand field around the Dy^{3+} ions affect the Ω_2 parameter, while Ω_4 and Ω_6 depend on the viscosity of the medium and rigidity of medium. The Ω_6 specifies the rigidity and a lower polarizability. Moreover, the determined Ω_6 value indicates strong ionic network coupling and also results merging the opposite similarity energy levels. This remains vital increase to emission intensity the Dy^{3+} ions and keeps the thermal stresses low in order to achieve the thermal equilibrium of the quantum efficiency. The large value of Ω_2 comparing with the Ω_6 indicates the large asymmetry around the Dy^{3+} ions and closes the binding of the ligand ions. Moreover, the Ω_2 value highly depends upon the sensitive transitions and

Table 3 Comparison of J-O intensity parameters (Ω_2, Ω_4, $\Omega_6 \times 10^{-22}$ cm^2) between OFSbBDy glasses and different reported Dy^{3+} ions doped glasses

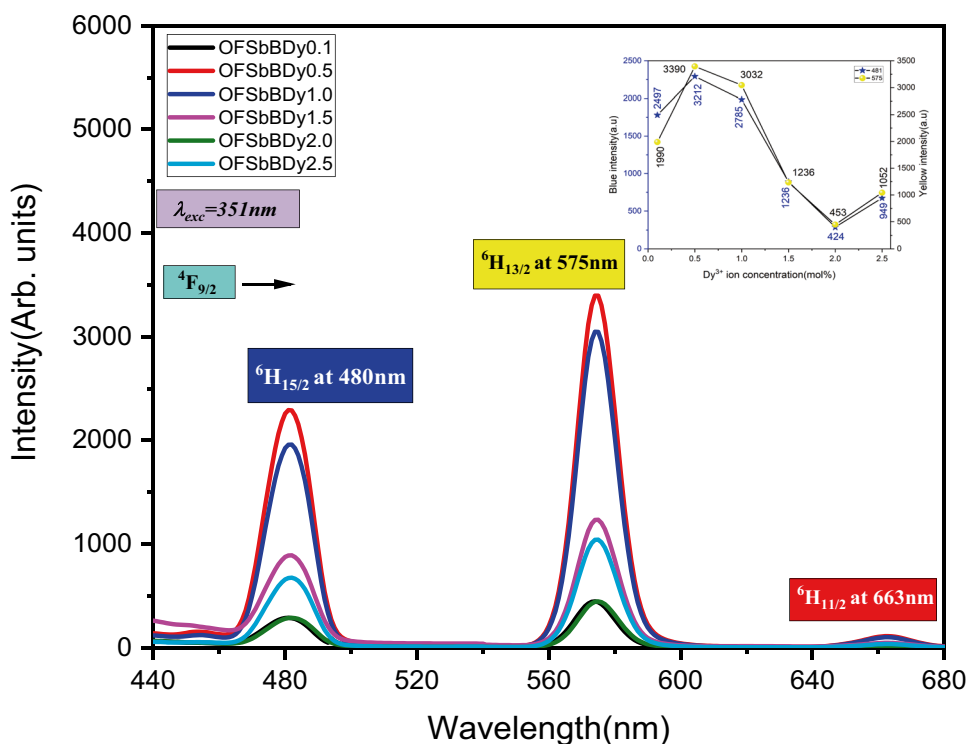| Glass system	Ω_2	Ω_4	Ω_6	Trend	References
OFSbBDy0.1	572.59	299.74	530.97	$\Omega_2 > \Omega_6 > \Omega_4$	Present work
OFSbBDy0.5	672.23	219.89	652.8	$\Omega_2 > \Omega_6 > \Omega_4$	Present work
OFSbBDy1.0	609.98	157.3	575.25	$\Omega_2 > \Omega_6 > \Omega_4$	Present work
OFSbBDy1.5	629.11	36.39	531.38	$\Omega_2 > \Omega_6 > \Omega_4$	Present work
OFSbBDy2.0	531.4	53.85	365.75	$\Omega_2 > \Omega_6 > \Omega_4$	Present work
OFSbBDy2.5	412.76	47.77	255.57	$\Omega_2 > \Omega_6 > \Omega_4$	Present work
LBGS0.5Dy	832	214	275	$\Omega_2 > \Omega_6 > \Omega_4$	[35]
Lead fluorophosphate glass	712	159	220	$\Omega_2 > \Omega_6 > \Omega_4$	[19]
oxyfluoride glass	641	102	225	$\Omega_2 > \Omega_6 > \Omega_4$	[36]
TSWD5	1220.2	264.4	337.5	$\Omega_2 > \Omega_6 > \Omega_4$	[37]
BTLN0.5D	632.9	171.5	114.1	$\Omega_2 > \Omega_6 > \Omega_4$	[38]
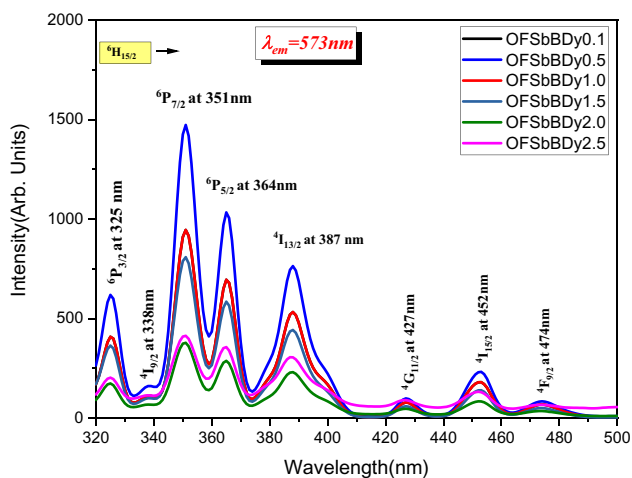
Fig. 5 The excitation spectra of Dy^{3+} ion doped OFSbB glass samples

provides the information on the nature of the Dy-O bonds. Higher oscillator strengths of hypersensitive transitions lead to maximum values of Ω_2. The prepared glasses typically have Ω_2 values that lies between in the range of Ω_6 and Ω_4 for the oxyfluoride glass. As we see that Ω_2 increases until OFSbBDy0.5 glass greater and confirming the high asymmetry ligand field around the Dy^{3+} ions of the prepared glass. The J-O values results are compared with published work which is shown in Table 3 [19, 35–38].

Photoluminescence Spectra

PL spectral studies of the Dy^{3+} ions doped OFSbB glasses were recorded and which are represented in the Figs. 5 and 6. Figure 5 The excitation spectra were in the range of 320 nm to 500 nm, and the emission spectra (Fig. 6) were in the range of 450 nm to 750 nm. At an emission wavelength of 573 nm, the peaks of the excitation bands located at 325, 338, 351, 364, 387, 427, 452, and 474 nm were related to transitions from $^4M_{17/2}$, $^6P_{7/2}$, $^6P_{5/2}$, $^4I_{13/2}$, $^4G_{11/2}$, $^4I_{15/2}$, and $^4F_{9/2}$. Amongst these transitions, the $^6H_{15/2} \rightarrow {}^6P_{7/2}$ band at 351nm was relatively more intense than the other transitions. The results of the two highly intense bands at 480 nm(blue), 575 nm (yellow) and one less intense band at 663nm (red) corresponding to the transitions from the excited level $^4F_{9/2} \rightarrow {}^6H_{15/2}$, $^4F_{9/2} \rightarrow {}^6H_{13/2}$ and $^4F_{9/2} \rightarrow {}^4H_{11/2}$ respectively. The Fig. 7 represents the variation of emission intensities of OFSbBDy0.5 glass excited at different excitation wavelengths. From the emission spectra, it is observed that luminescence intensity increases up to 0.5 mol% of Dy_2O_3 and decreases beyond because of concentration quenching effect. The concentration quenching effect is the result of the Dy-Dy distance, which occurs with increasing Dy_2O_3 concentration. The reduction in Dy-Dy distance shows resonant energy transfer (RET), which is otherwise called "energy migration" and the cross-relaxation (CR) energy transfer process between Dy^{3+}
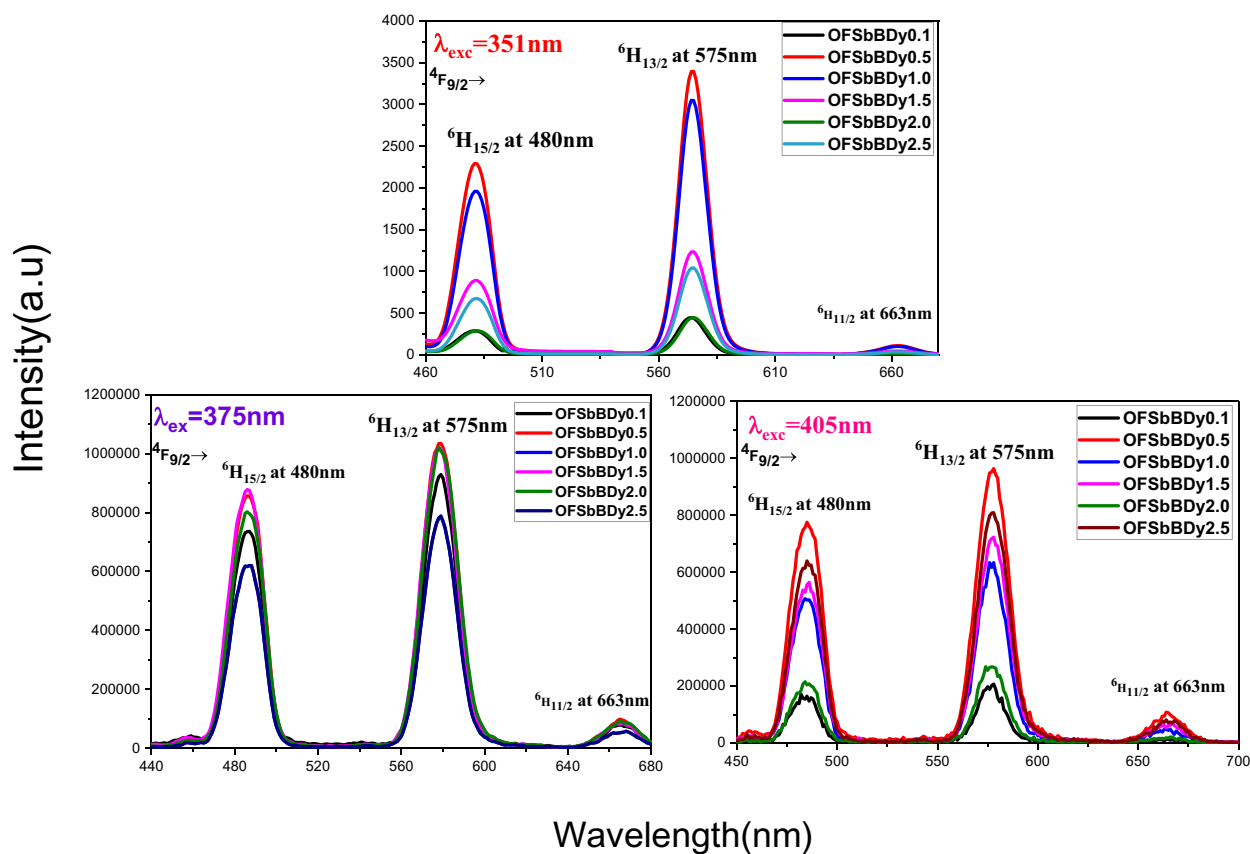
Fig. 6 The emission spectra of Dy^{3+} ion doped OFSbB glass at an excitation wavelength 351 nm. The inset shows the Yellow-blue (Y/B) intensity ratio of Dy^{3+} ions doped OFSbB glasses

Fig. 7 The emission spectra of Dy^{3+} ion doped OFSbB glass at an excited at 351 nm, 375 nm and 405 nm wavelengths

donor ions and acceptor ions. In Fig. 8, the Dy^{3+} ions partial energy level diagram and the RET, which corresponds to the PLE and PL transitions ($^6H_{15/2} \rightarrow {}^6H_{15/2}: {}^4F_{9/2}$) as well as CR ($^6H_{15/2} \rightarrow {}^6F_{5/2}: {}^6F_{9/2}$), ($^4F_{9/2}: {}^6H_{15/2} \rightarrow {}^6F_{3/2}: {}^6F_{11/2}$) [39].

Among all the above-mentioned transitions of the PL spectra, the transition at $^4F_{9/2} \rightarrow {}^6H_{15/2}$ is allowed magnetic dipole and the transition at $^4F_{9/2} \rightarrow {}^6H_{11/2}$ is forced electric dipole in nature [40]. The relationship between these two transitions indicates the nature of the dysprosium-oxygen bond by determining the ratio of yellow to blue, the degree of covalence between Dy-O ions increases with its value. In addition, for studying the symmetry shifts in Dy^{3+} ions, an important parameter is the yellow-to-blue intensity ratio (Y/B) which is shown inset of Fig. 6. The Y/B intensity ratios were 1.11, 1.56, 1.48, 1.38, 1.55, and 1.54, corresponding to the OFSbBDy0.1, OFSbBDy0.5, OFSbBDy1.0, OFSbBDy1.5, OFSbBDy2.0 and OFSbBDy2.5 glasses. The increase in the Y/B ratio indicated an increase in the covalent nature of the Dy-O bond. This indicates higher structural disorder around the Dy^{3+} ions [26, 27].

Radiative Properties

Following the expressions reported in the literature [41]. The radiative properties have been calculated using J-O Parameters

which includes effective bandwidths, radiative lifetimes (τ_R), radiative transition probabilities (A_R), Stimulated emission cross-sections (σ_{se}) and branching ratios (β_{exp}). The A_R values influenced by the J-O intensity parameters and the energy gap between the initial and terminal levels, to determine the radiative relaxation of an excited state to all its lower levels

$$\tau R = \frac{1}{A_\tau(\psi J)} \tag{7}$$

where A_T denotes the total probability of transition which is the summation of transition probability values for a potential transition. The branching ratio (β_R) is the basic parameter for the designing the laser since it portrays the chance of accomplishing the stimulated emission from any specific transition. The value for the potential laser activity must be greater than 0.5. The following expression can be used to determine the value of R from the total transition probability (A_T) that corresponds to the emission and excited level to the lower level

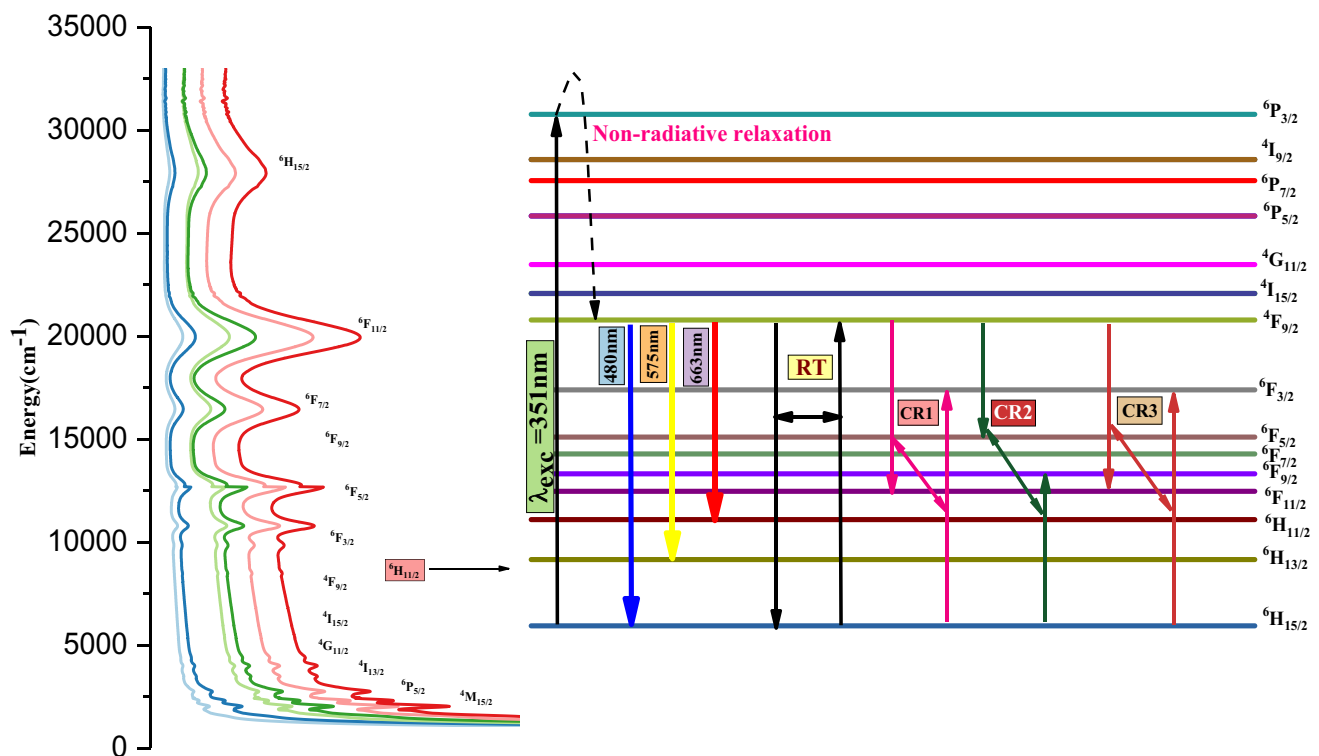$$\beta_R = \frac{A_R(\psi J, \psi' J')}{A_T(\psi J)} \tag{8}$$

Fig. 8 The partial energy level diagram of Dy^{3+} ions doped OFSbB glass samples

The higher branching ratio of the $^4F_{9/2} \rightarrow {^6H_{13/2}}$ shift among the observed emission shifts indicates that it is suitable for its lasing action. From the Table 5, the observed β_{exp} values for each prepared glasses tend to be $^6H_{13/2} > {^6H_{15/2}} > {^6H_{11/2}}$ which indicates that yellow emission is predominant. As a result, the prepared glasses are promising materials for visible yellow laser applications. Laser execution is highly dependent upon the σ_{se} which lies between the primary level (ΨJ) and the concluding level ($\Psi'J'$) with possibility A_R is calculated as follows

$$\sigma_{se}(\psi J, \psi'J') = \left(\frac{\lambda_p^4}{8\pi \sigma n^2 \Delta\lambda_p}\right) A_R(\psi J, \psi'J') \qquad (9)$$

where, λ_P is the emission lines peak wavelength and $\Delta_{\lambda eff}$ is the effective bandwidth of the emission band, The effective bandwidth is determined by integrating the luminescence line's intensity and dividing it by the intensity at the peak wavelength. The outcome for the radiative properties is recorded in Table 4. The optical gain bandwidth ($\sigma_{se} \times \Delta\lambda_p$) and optical gain ($\sigma_{se} \times \tau_R$) values fundamental for manufacturing lasers and optical materials [42]. For the $^4F_{9/2} \rightarrow {^6H_{13/2}}$ transition, OFSbBDy0.5 glass has relatively higher values for gain bandwidth and optical gain parameters than the other prepared glasses which is shown in Table 5, This indicates the suitability of OFSbBDy0.5 glass for the visible laser and fiber amplifiers. [30, 35, 43–49].

Photoluminescence Decay Analysis

With an excitation wavelength of 351nm and an emission wavelength of 575nm, the time decay profile for all the as

Table 4 The Radiative transition probability (A^{s-1}), radiative branching ratios (β_R) and stimulated emission cross-section (σ_{se}) (10^{-22} cm^2) for the emission transitions of Dy^{3+} ions doped OFSbB glasses

Glass system	Transition	A	β_R	σ_{SE}
OFSbBDy0.1	$^4F_{9/2} \rightarrow {^6H_{11/2}}$	288	0.05	0.325
	$^4F_{9/2} \rightarrow {^6H_{13/2}}$	3254	0.573	2.724
	$^4F_{9/2} \rightarrow {^6H_{15/2}}$	1528	0.269	0.886
OFSbBDy0.5	$^4F_{9/2} \rightarrow {^6H_{11/2}}$	321	0.05	0.366
	$^4F_{9/2} \rightarrow {^6H_{13/2}}$	3707	0.577	3.139
	$^4F_{9/2} \rightarrow {^6H_{15/2}}$	1775	0.276	1.041
OFSbBDy1.0	$^4F_{9/2} \rightarrow {^6H_{11/2}}$	287	0.051	0.329
	$^4F_{9/2} \rightarrow {^6H_{13/2}}$	3246	0.578	2.764
	$^4F_{9/2} \rightarrow {^6H_{15/2}}$	1533	0.273	0.904
OFSbBDy1.5	$^4F_{9/2} \rightarrow {^6H_{11/2}}$	275	0.054	0.319
	$^4F_{9/2} \rightarrow {^6H_{13/2}}$	3002	0.589	2.586
	$^4F_{9/2} \rightarrow {^6H_{15/2}}$	1533	0.263	0.8
OFSbBDy2.0	$^4F_{9/2} \rightarrow {^6H_{11/2}}$	223	0.058	0.263
	$^4F_{9/2} \rightarrow {^6H_{13/2}}$	2257	0.595	1.976
	$^4F_{9/2} \rightarrow {^6H_{15/2}}$	905	0.238	0.549
OFSbBDy2.5	$^4F_{9/2} \rightarrow {^6H_{11/2}}$	176	0.062	0.209
	$^4F_{9/2} \rightarrow {^6H_{13/2}}$	1668	0.59	1.467
	$^4F_{9/2} \rightarrow {^6H_{15/2}}$	631	0.223	0.384

Table 5 Emission peak wavelength(λ_p) (nm), effective band width ($\Delta\lambda_p$) (nm), stimulated emission cross-section (σ_{se}) (10^{-22} cm^2), gain band width (σ_{se} x $\Delta\lambda_p$) (10^{-28} cm^3) and optical gain (σ_{se} x τ_R) (10^{-25} cm^2 s) for the emission transitions of Dy^{3+}ions doped OFSbB glasses

Glass code	$^4F_{9/2} \rightarrow {}^6H_{15/2}$ (Blue)					$^4F_{9/2} \rightarrow {}^6H_{13/2}$ (Yellow)					$^4F_{9/2} \rightarrow {}^6H_{11/2}$ (Red)				
	$\Delta\lambda_P$	σ_{SE}	σ_{SE} x $\Delta\lambda_P$	τ_R	σ_{SE} x τ_R	$\Delta\lambda_P$	σ_{SE}	σ_{SE} x $\Delta\lambda_P$	τ_R	σ_{SE} x τ_R	$\Delta\lambda_P$	σ_{SE}	σ_{SE} x $\Delta\lambda_P$	τ_R	σ_{SE} x τ_R
OFSbBDy0.1	3.84	0.886	3.402	176	1.559	5	2.724	13.62	176	4.794	5.25	0.325	1.706	176	0.572
OFSbBDy0.5	5	1.041	5.205	155	1.613	5.55	3.139	17.421	155	4.865	6.25	0.366	2.287	155	0.567
OFSbBDy1.0	5	0.904	4.52	178	1.609	3.84	2.764	10.613	178	4.919	4.17	0.329	1.371	178	0.585
OFSbBDy1.5	5.55	0.8	4.44	196	1.568	5	2.586	12.93	196	5.068	4.55	0.319	1.451	196	0.625
OFSbBDy2.0	5	0.549	2.745	263	1.443	3.57	1.976	7.054	263	5.196	5.55	0.263	1.459	263	0.691
OFSbBDy2.5	5	0.384	1.92	353	1.355	4.54	1.467	6.660	353	5.178	5.55	0.209	1.159	353	0.737

prepared samples that correspond to the $^4F_{9/2}$ state was taken into consideration. As can be seen in Fig. 9, the time decay profile of each Dy^{3+} ions doped glass sample contained only one exponential and the estimated values for the decay time. Due to the concentration quenching effect, it was discovered

that the time decay values decreased as Dy^{3+} ions concentration increased [50]. Using the following the expressions reported in the literature [41], the experimental lifetimes of the as prepared glasses are calculated by fitting the decay profiles by using following equation
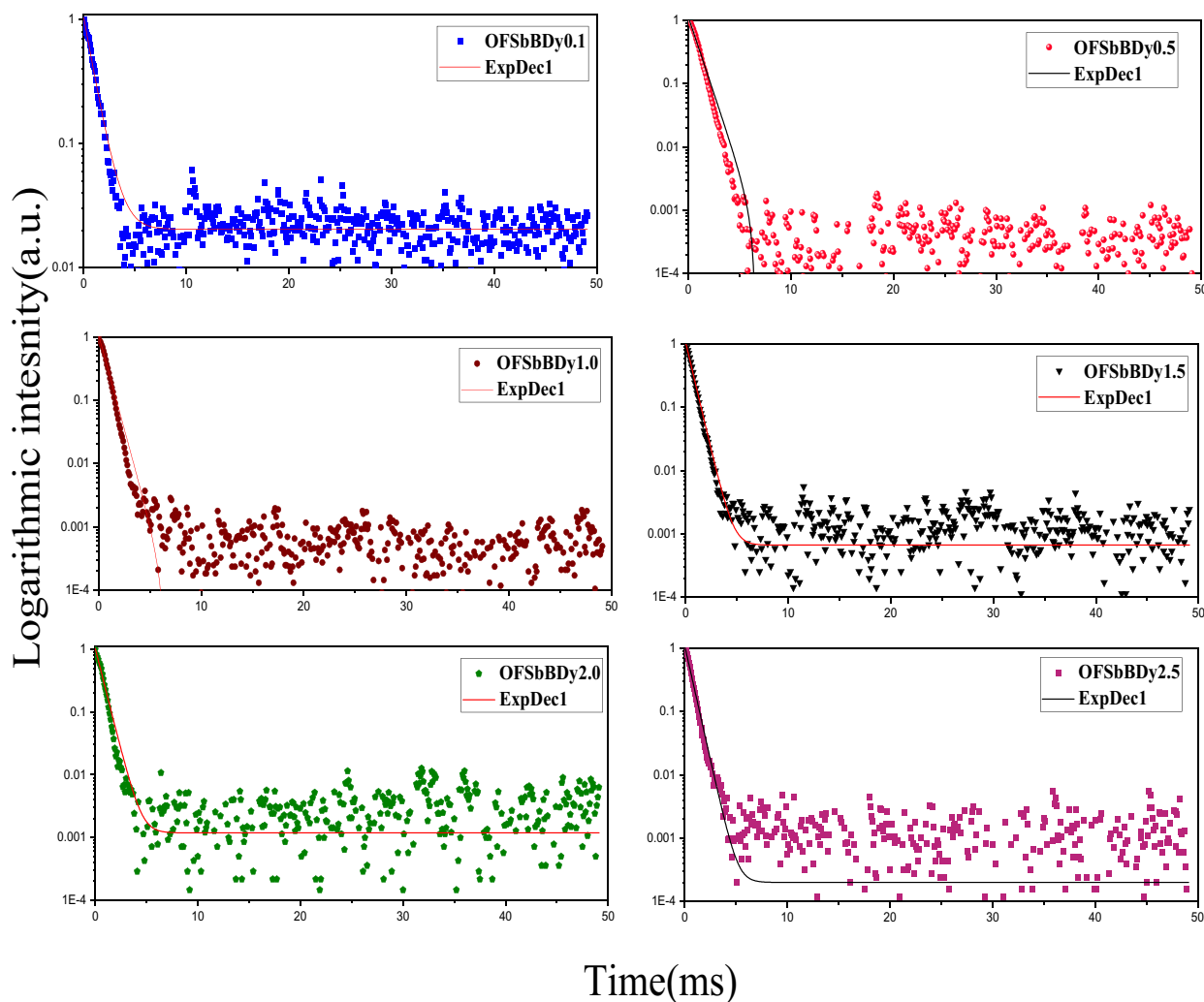

Fig. 9 The decay curves of Dy^{3+} ions doped OFSbB glass samples

$$I_t = I_o e^{\frac{t}{\tau_{exp}}} \tag{10}$$

where I_t and I_o represent the intensities of emission for decay curves at $t=0$ and $t=t$ respectively. With an increase in the concentration of the Dy^{3+} ions, the experimental lifetime values of the $^4F_{9/2}$ level are 140, 135, 115, 105, 95 and 84(μs) corresponding to OFSbB0.1, OFSbB0.5, OFSbB1.0, OFSbB1.5, OFSbB2.0, and OFSbB2.5, respectively. The determined radiative lifetimes are opposing more from the experimental lifetimes which is due to non-radiative transition in the glass. The quantum efficiency (η) is the ratio of number photons emitted to the photons observed. For RE ions doped glasses, the quantum efficiency is expressed as

$$\eta = \frac{\tau_{exp}}{\tau_R} x 100 \tag{11}$$

The η values are decrease with increase in Dy^{3+} ions concentration due to increase of non-radiative transition rates. These rates can be calculated by difference of inverses of experimental and radiative lifetime value:

$$W_{NR} = \frac{1}{\tau_{exp}} - \frac{1}{\tau_{rad}} \tag{12}$$

The determined values of the quantum efficiency and W_{NR} are of prepared glasses are tabulated in the Table 6 and compared with reported values. The W_{NR} values of OFSbBDy0.5 are minimum which is evidently the OFSbBDy0.5 possess higher stimulated emission cross section and quantum efficiency.

Commission Intermediate de l' Elcairage (CIE) Chromaticity Coordinates.

The combination of two intense emissions (blue and yellow) in the visible region can generate white light, which was analyzed using the Commission Internationale de I'Eclairage (CIE) to obtain color coordinates. Slightly emission color

Table 6 Experimental lifetimes (τ_{exp}), radiative lifetimes (τ_R), quantum efficiency (η) and non-radiative decay rates (W_{NR}) of $^4F_{9/2} \rightarrow {}^6H_{13/2}$ transition of OFSbBDy glasses along with reported other glasses.

Glass system	τ_{exp}(μs)	τ_R (μs)	η(%)	W_{NR} (s⁻¹)	References
OFSbBDy0.1	140	176	79.54	1461	Present work
OFSbBDy0.5	135	155	87.09	955	Present work
OFSbBDy1.0	115	178	64.6	3077	Present work
OFSbBDy1.5	105	196	53.57	4421	Present work
OFSbBDy2.0	95	263	36.12	6724	Present work
OFSbBDy2.5	84	353	23.79	9071	Present work
BTKA0.5D	461	1160	39.4	1310	[47]
TWZDy0.5D	145	-	54	447	[48]
BTLNDy0.5	414	1043	45	1457	[38]
DZCTFB0.5	340	515	66	999	[49]

is labeled using color identical function (X, Y, Z) besides the color of the spectral power density P(λ) must match the simulation for each of the three primary colors. The tristimulus values are used to calculate the chromaticity coordinates x and y using the equations.

$$x = \frac{X}{(X+Y+Z)} ... ; ... = \frac{Y}{(X+Y+Z)} \text{ and } z = \frac{Z}{(X+Y+Z)} \tag{13}$$

As a result, the coordinates for white-light emission are close to the center of the chromaticity diagram. Plots of the CIE chromaticity diagram was made for each prepared glass sample in relation to various excitation wavelengths. Figures 10 and 11 depicts the CIE diagram for the OFSbBDy0.5 sample with various excitations, as well as the CIE diagram for all samples with an excitation wavelength of 351nm. In comparison to the other excitations, the OFSbBDy0.5 sample produce the significant near-white light emission for the 351nm excitation. The emission from Dy^{3+} ions-doped glasses as depicted by the corresponding CIE coordinates (x,y) in Table 7 which suggests their potential use as materials for w-LEDs applications.

McCamy proposed a third-order polynomial equation for calculating CCT from CIE 1931 color coordinates in order to examine the quality of any light source in terms of correlated color temperature. This equation reduces the specification of white color from two dimensions (CIE diagram) to one dimension [51].
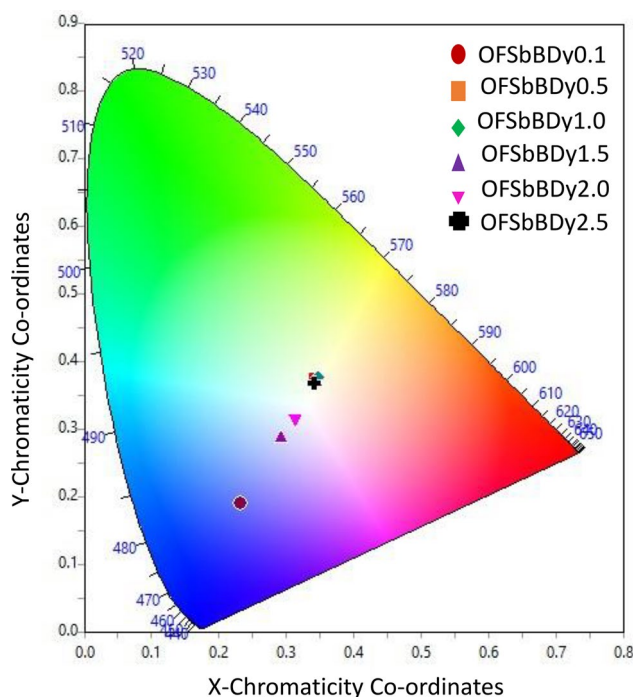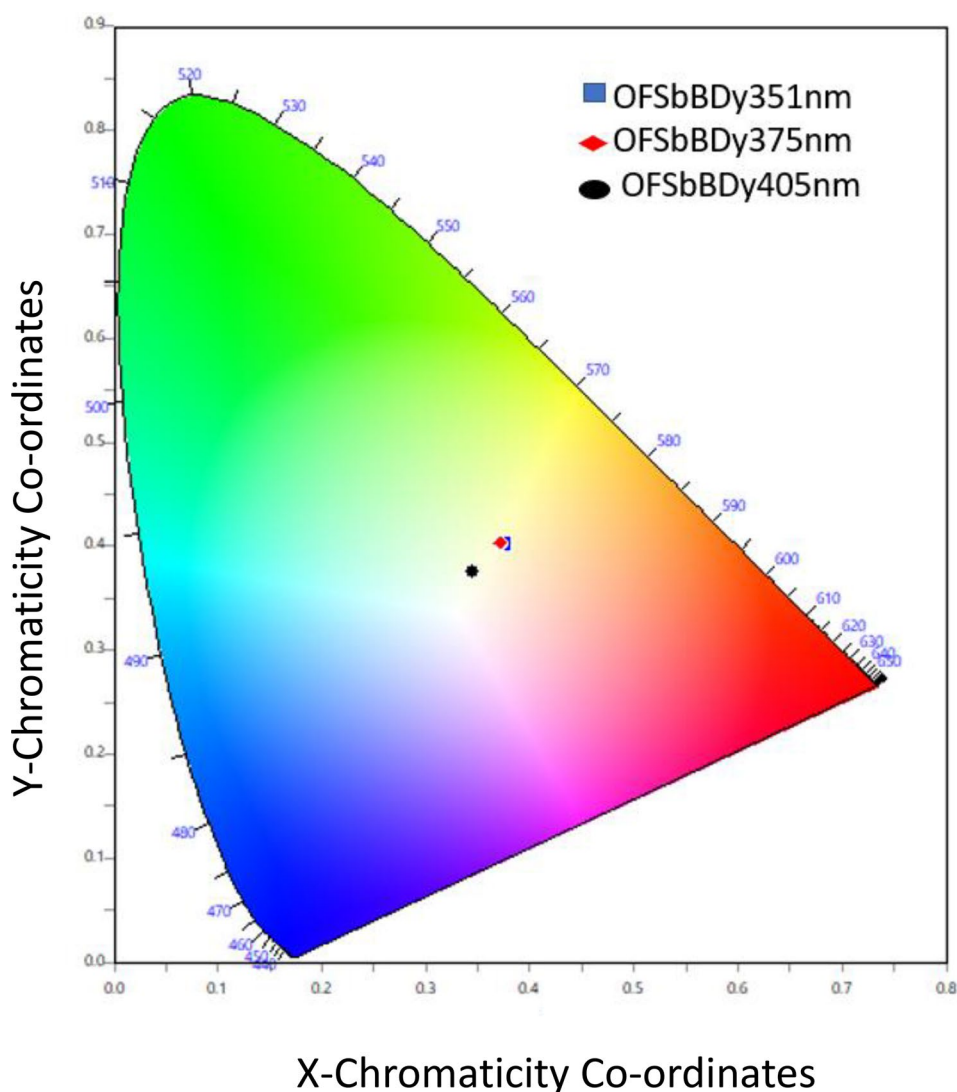

Fig. 10 CIE 1931 chromaticity diagram of Dy^{3+} ions doped OFSbB glass samples

Fig. 11 CIE profile for Dy series at different excitation wavelengths

$$CCT = -49n^2 + 352n^2 - 682n + 5520.33 \qquad (14)$$

The reciprocal slope is given by $n = (x - x_e)/(y - y_e)$ and the convergence epicenter is given by $x_e = 0.332$, $y_e = 0.186$ respectively. In most cases, the CCT values can be used to identify white light. If CCT value ≤ 3700 K, it corresponds to emission which represent warm and the emission color is pure for CCT values between 3700 and 5000K, it is considered as pure and below 5000 K, it is considered cooler. Hence, it is noteworthy that the CCT values estimated in Tables 8 and 9 for the OFSbBDy0.5 sample excited at wavelength of 351nm were found to be pure white light.

Gamma Radiation Shielding Properties

Web-based software.

Photon shielding and dosimetry (PSD) software is a user-friendly online software program accessible on https://phy-x.net/PSD, which was established used for to calculate the parameters related to shielding and dosimetry. Depending on the number of calculations, it produces results on a NodeJS platform in a reasonable amount of time. The software generates data on radiation shielding parameters by selecting two energies that have been defined in the software namely 0.0015MeV-15MeV & 1keV to 100GeV. In addition, the software includes a number of well-known radioactive sources (^{22}Na, ^{55}Fe, ^{60}Co, ^{109}Cd, ^{131}I, ^{133}Ba, ^{137}Cs, ^{152}Eu, & ^{241}Am), as well as their energies and some characteristic like K-shell X-ray energies for Rb, Mo, Ag, Cu, Ba & Tb elements, which the user can select. The parameters include the mass attenuation coefficient, linear attenuation coefficient, half-value layer, tenth value layer, effective atomic number, mean free path, effective conductivity, electron density, energy absorption, and exposure buildup factor.

Table 7 CIE Chromaticity coordinates (X and Y) and Y/B ratios of Dy^{3+} ions doped OFSbB glasses excited at 351nm wavelength.

Glass Code	Y/B ratio	Chromaticity co-ordinates		CCT(K)
		x	y	
OFSbBDy0.1	1.11	0.2826	0.2992	9225
OFSbBDy0.5	1.56	0.3434	0.3724	5122
OFSbBDy1.0	1.48	0.3477	0.3769	4989
OFSbBDy1.5	1.38	0.2921	0.2871	8844
OFSbBDy2.0	1.55	0.3131	0.3161	6589
OFSbBDy2.5	1.54	0.3422	0.3674	5152

Table 9 Comparison of CIE Chromaticity coordinates (X and Y) and Y/B ratios of OFSbBDy glasses with other reported Dy^{3+} doped glasses.

Glass code	Y/B	Chromaticity coordinate		CCT(K)	References
		x	y		
OFSbBDy0.5	1.56	0.34	0.37	5122	PW
LBGS0.5Dy	1.66	0.41	0.42	3621	[35]
BTSrZofDy0.5	1.76	0.32	0.35	5841	[46]
BiNFB0.5Dy	-	0.37	0.38	4144	[44]
NbFSDy	0.82	0.33	0.37	5593	[30]

Gamma Ray-radiation Shielding Parameters Fundamental Relations: By following the Beer-Lambert's law, reduces the intensity of the beam when a material with the thickness "x" is placed in the path of a monoenergetic x-ray and gamma ray beam.

$$I = I_0 e^{-\mu x} \tag{15}$$

where I_0 and I are the intensities prior to and following attenuation, respectively; x is the thickness of the sample; and μ is the Linear Attenuation Coefficient cm^{-1} (LAC). LAC is important because it describes the material interaction with radiation and it quantifies how much radiation is absorbed/scattered as it passes through the material.

The mass attenuation coefficient (MAC) is an important parameter for calculating the radiation shielding parameters. Understanding behavior of radiation and developing new applications for radiation-based new technologies require the MAC. It is used to evaluate the probability of interaction of the photons with the glass sample. It is theoretically calculated by using mixture rule [52].

$$MAC_{(\mu_m)} = \mu/\rho = \Sigma_i w_i (\mu/\rho)_i \tag{16}$$

Here, $(\mu/\rho)_i$ and w_i are the photon mass attenuation coefficient and weight fraction of the element and the "i" is obtained from the aforementioned software.

The material's thickness level in cm is referred to as the half-value layer (HVL). which can reduce the incoming radiation to half of its initial value [53, 54]. The low HVL value implies many interactions of gamma rays with the sample; thus, the prepared sample has better gamma ray shielding effectiveness. HVL is likewise to another parameter called the Mean Free Path (MFP), which characterizes the typical distance went by a photon in the medium before the interaction happens. The following equations can be used to determine the HVL and MFP:

$$HVL = \frac{0.693}{\mu} \tag{17}$$

and,

$$MFP = \frac{1}{\mu} \tag{18}$$

where, μ is the Linear Attenuation Coefficient "which is equal to the MAC x density of the prepared sample."

The effective atomic number (Z_{eff}) was used to calculate the shielding characteristics of the materials. Z_{eff} can be calculated using the following equation [55, 56].

$$Z_{eff} = \frac{\sigma_{t,a}}{\sigma_{t,el}} \tag{19}$$

Here,

$$\sigma_{t,a} = \frac{\mu/\rho}{N_A \Sigma_i (\frac{w_i}{A_i})} \cdots ; \cdots \sigma_{t,el} \frac{1}{N_A} \Sigma_i \frac{f_i A_i}{Z_i} (\mu/\rho)$$

Table 8 CIE Chromaticity coordinates (X and Y) and Y/B ratios of OFSbBDy0.5 glasses at different excitation wavelengths.

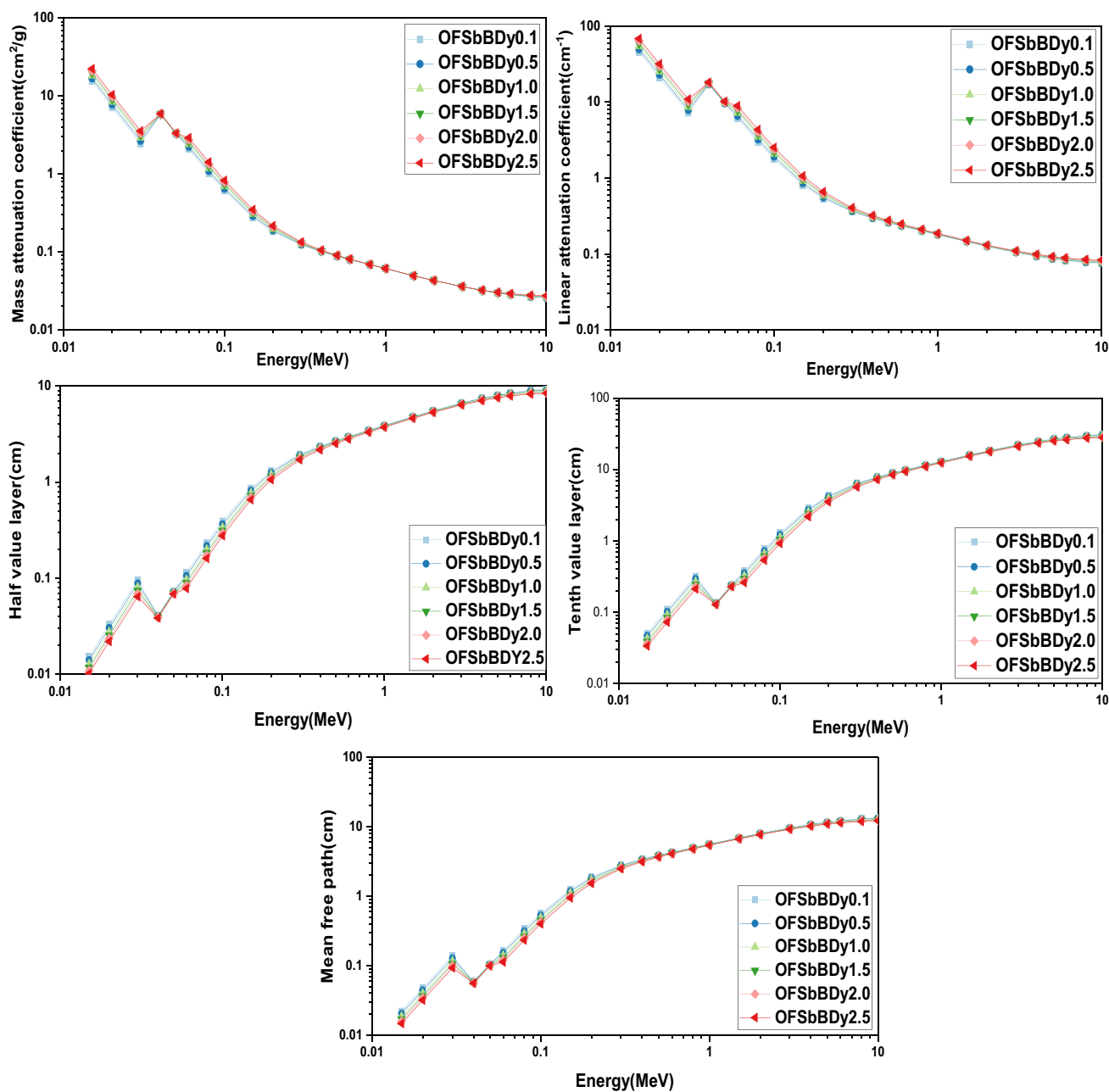| Glass Code	Excitation(nm)	Y/B ratio	Chromaticity Co-ordinates		CCT(K)
			x	y	
OFSbBDy0.5	351	1.56	0.3434	0.3724	5122
OFSbBDy0.5	375	0.116	0.3746	0.4026	4320
OFSbBDy0.5	405	1.24	0.3717	0.4031	4397

Fig. 12 The variation of mass attenuation coefficient, linear attenuation coefficient, half value layer, tenth value layer, Mean free path of the prepared OFSbBDy glasses

Where, A_i is atomic weight of the ith element, N_A is Avogadro's number, f_i & Z_i are fractional abundance & atomic number respectively of the ith element.

In high-energy radiation fields, where the radiation buildup can be significant, exposure buildup factor (EBF) plays crucial role. Also, the EBF is an essential parameter for estimating the distribution of photons in an illuminated medium [57]. The ability of the EBP is to predict the dose rate at a specific point behind a shield. The EBP was calculated using the following steps:

(a) Finding the equivalent atomic number (Zeq)
(b) Finding the G-P fitting parameters (b,c,a,Xk & d)
(c) Finding the exposure buildup factor EBF.

Fig. 13 Mean Free Path for prepared glass in comparison with ordinary concrete and zinc oxide soda lime silica
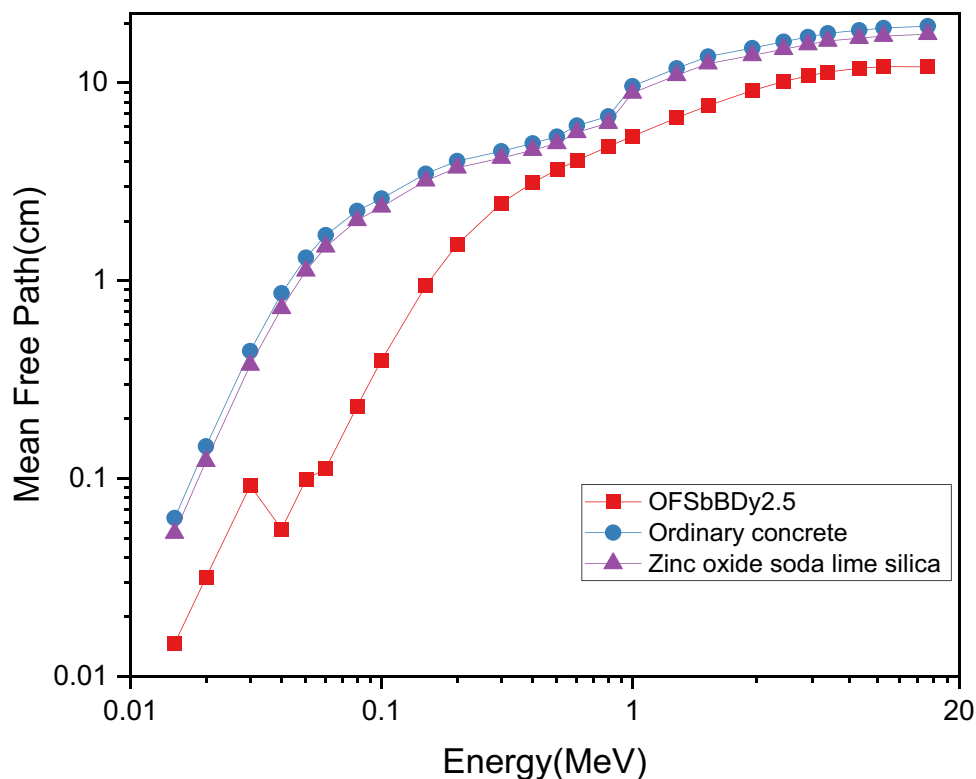
Results

The gamma-ray shielding parameters of the prepared glasses were measured for incident photon energy 0.015-15MeV

Figure 12. The variation of MAC, LAC, HVL, TVL and MFP of the prepared OFSbBDy glasses. The decrease with increasing photon energy is owing to attenuators deeper penetration of photons. The fact that the change of the

Fig. 14 Comparison of Mass Attenuation Coefficient (MAC) (cm^2/g) and Half Value Layer (HVL) (cm) at 1173 keV of 2.5 mol% doped OFSbB glass with different concretes
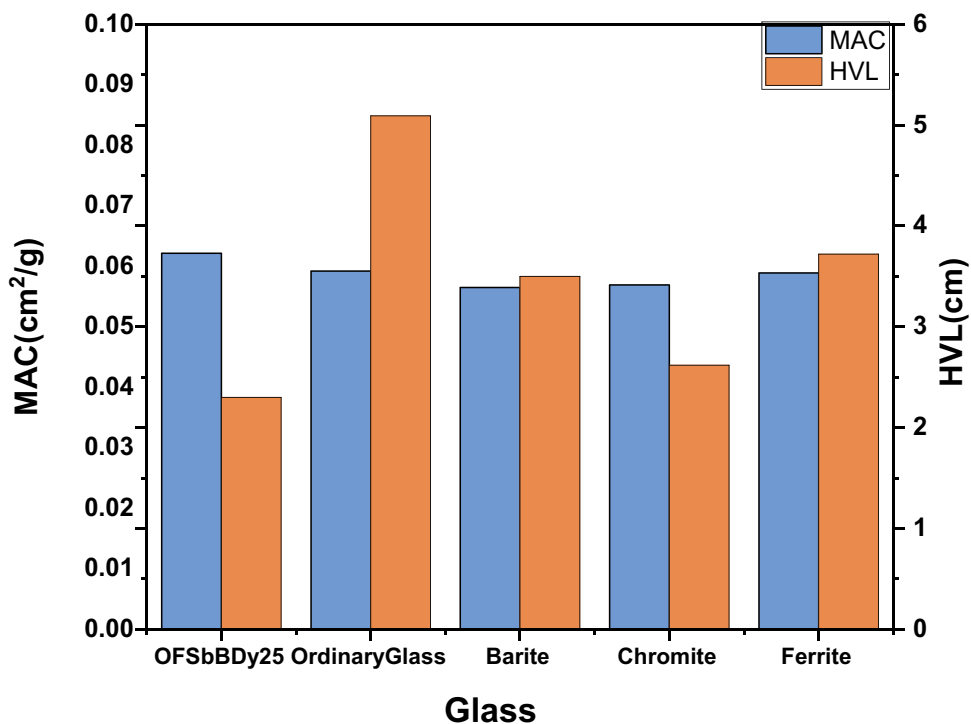
Fig. 15 The variation of the effective atomic number (Z_{eff}) with the photon energy for the OFSbBDy glasses
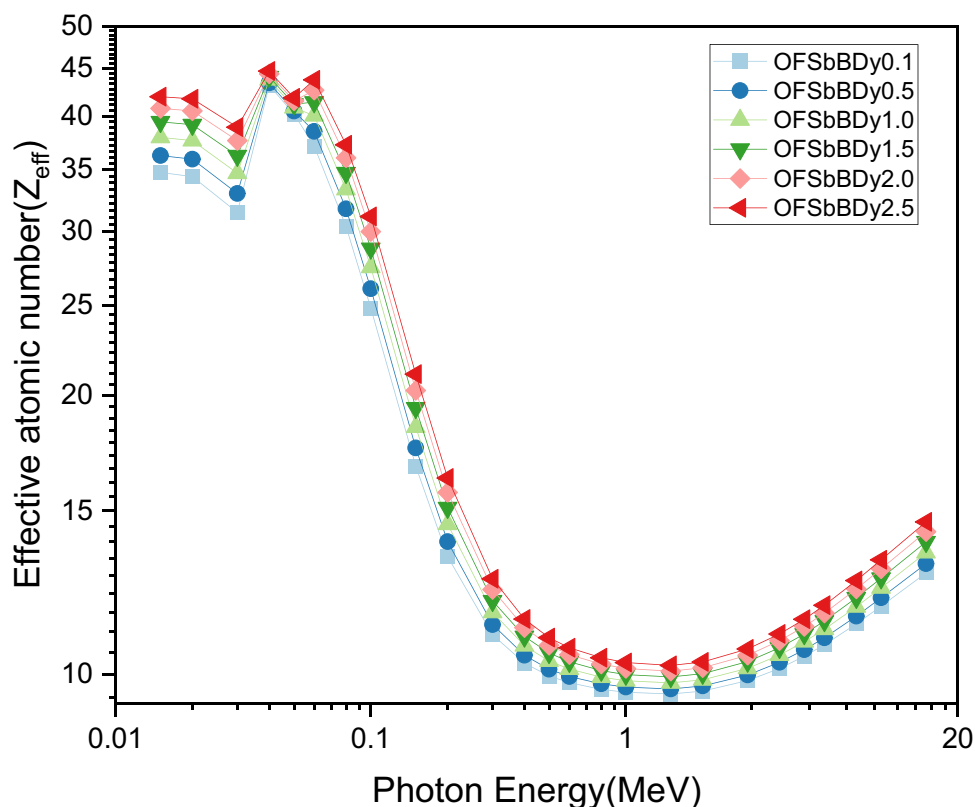
MAC values seen that the swift decrease at the range of 0.02–0.5MeV is due to photoelectric absorption (PE) which becomes dominant process. After a slight decrease in the range of 0.5-3MeV MeV, Compton scattering (CS) becomes the dominant process. Subsequently, the minor increase in the photon energy range of 4-15MeV was due to the pair production process (PP). The linear attenuation coefficient of the prepared glasses, which has a higher value in the lower-energy region and a lower value in the higher-energy region. The LAC results in a trend similar to of that the MAC. Hence, OFSbBDy2.5 glass had a higher shielding effectiveness than the others.

The HVL in the lower region is the same for all the samples; thereafter, an increase in the value, peak is observed in the range of 0.02–0.5MeV for all glass samples. The TVL results which exhibits the same trend as the HVL. The MFP exhibits a behavior similar to that of the HVL and TVL, which are independent in the lower region (0.01MeV) and dependent in the higher region(15MeV). The Mean Free Path values for the prepared glass samples, ordinary concrete [58], and zinc oxide soda-lime silica glass [59] are compared in Fig. 13. This clearly indicates that the prepared glass samples possessed better shielding properties. Furthermore, the results of MAC and HVL at 1173keV are also compared to those of other radiation shielding concretes (ordinary glass, barite, chromite and Ferrite) in order to provide a more conclusive picture of studied glasses attenuation capacity and the results are shown in Fig. 14 the OFSbBDy2.5 glass has

a lower value than concrete, indicating that OFSbBDy glasses are better protection form γ-radiation.

For all prepared glass samples, the high Z_{eff} value is observed in low region and decreased with increases photon energy. Z_{eff} increases with increase in Dy_2O_3 content and it results that OFSbBDy2.5 can absorb high photon energy.
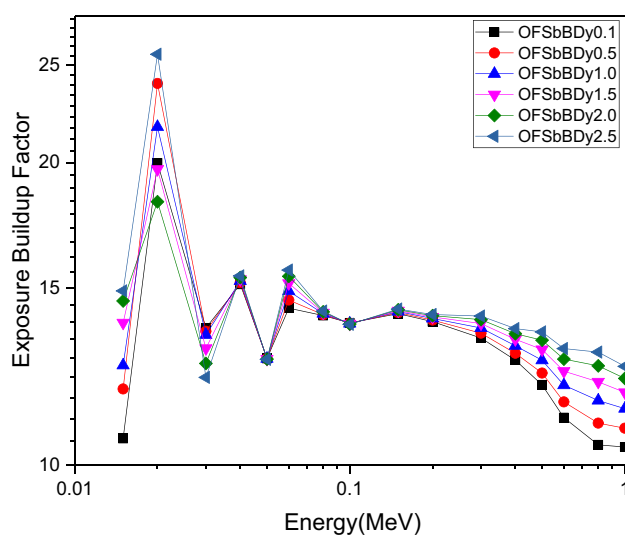

Fig. 16 The variation of the Exposure build factor with the photon energy for the OFSbBDy glasses

Figure 15 shows the variation of the effective atomic number (Z_{eff}) with the photon energy for the OFSbBDy glasses. From the Fig. 15 we can observe that high Z_{eff} was observed at 0.04MeV, where the photoelectric effect and predominant scattering is Compton. The interaction of cross-section, which is directly proportional to the atomic(Z) number, is the Compton scattering process. Consequently, it explains the change of the value in the lower region of Z_{eff}. However, Z_{eff} reaches its minimum value in the range of 1MeV to 5MeV. Finally, it remains constant after increase in photon energy hence the prepared glasses are competent shielding materials.

Figure 16 represents the variation of the Exposure build factor with the photon energy for the OFSbBDy glasses. Figure 17 shows the EBF values in the lower range (0.015–0.3MeV) are most unity for different penetration depths. As we observed that the sharp peak in the EBF values which can be attributed of k-edge absorption of the glass continents. The graph makes it abundantly clear that the prepared glasses' EBF increase with
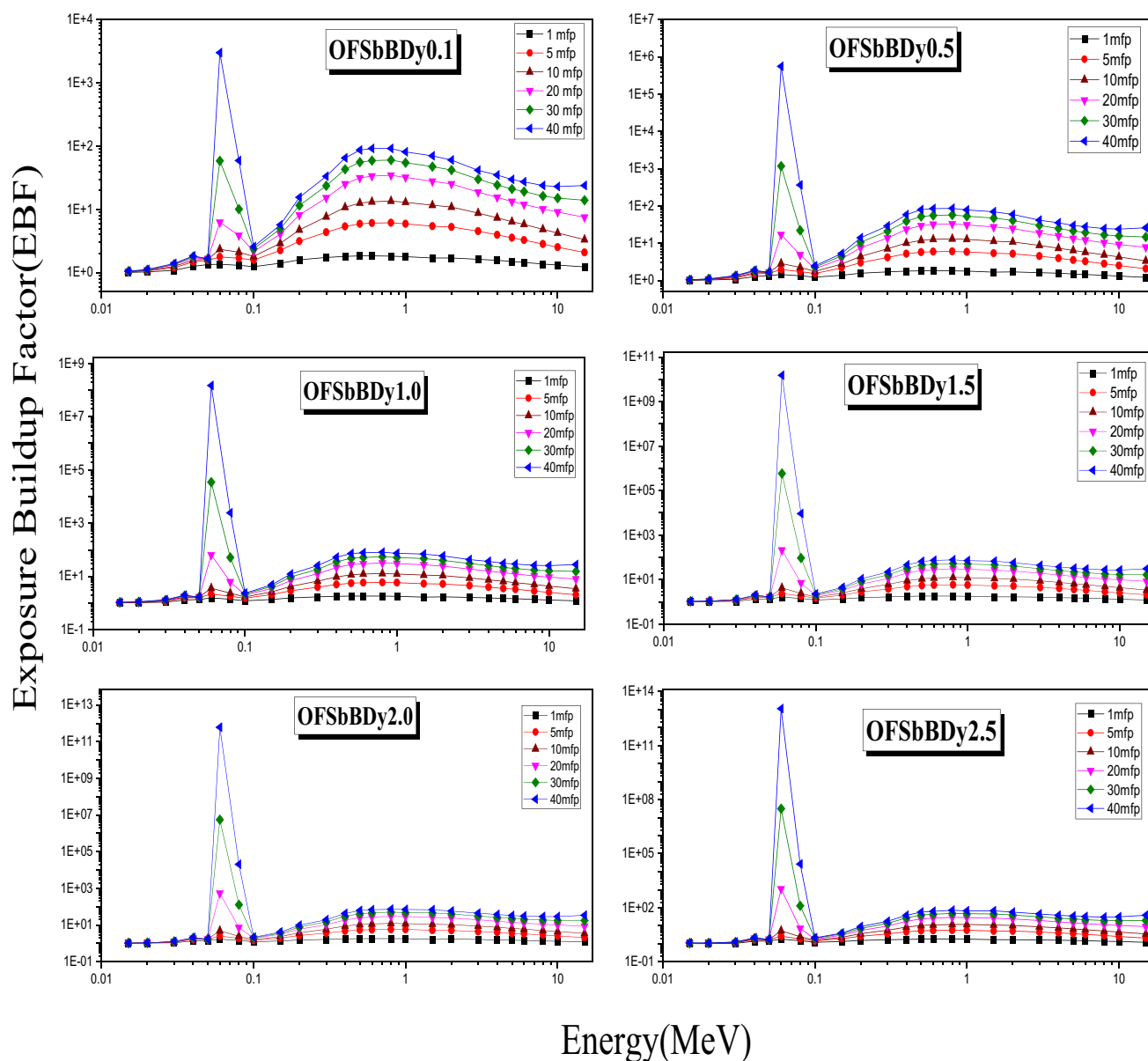

Fig. 17 The variation of the Exposure build factor with the photon energy for the OFSbBDy glasses

the mean free path. This also results increase of scattering events in target medium. Hence it results in large EBF values.

Conclusion

A series of Dy^{3+} ions doped antimony-oxyfluoro-borate glasses with a composition of $60B_2O_3$-$10Sb_2O_3$-$10Al_2O_3$-$10NaF$-(10-x) LiF-xDy_2O_3(x=0.1,0.5,1.0,1.5,2.0,2.5mol%) were prepared by using the conventional melt quenching method in this study. Various characterization methods, including UV–Vis-NIR, FTIR, luminescence, time decay. The non-metallic nature of NBO and glasses is the result of significant changes in a number of physical parameters brought about by the incorporation of Dy^{3+} ions into the host. UV–Vis-NIR absorption spectra also reveals the other host-dependent transitions and an intense peak that is associated with a hypersensitive transition. The Judd–Ofelt theoretical calculations were used to determine the radiative parameters and efficiency. From the J-O analysis, it was found that the J-O parameters follow the order$(\Omega_2 > \Omega_6 > \Omega_4)$. The optical bandgap analysis was estimated using Tauc's method. Emission studies have been analyzed using the excitation wavelengths from 351 to 575nm. The glass containing 0.5mol% of Dy^{3+} ions produced intense light-like emission when excited at 351nm wavelength. In general, Dy^{3+} ions incorporated antimony-oxyfluoroborate glasses are potential candidates for white light emission applications. The radiation shielding parameters of the prepared OFSbBDy glasses were studied at various photon energies (0.015MeV-15MeV) using PSD software. The MAC, LAC, HVL, TVL, MFP of the prepared glasses results same trend. The prepared glass OFSbBDy2.5 sample is capable of better radiation absorption glasses than the ordinary concrete and some other glass systems. Hence the prepared glass samples are good for shielding materials as well as optical applications.

Author Contributions All authors contributed to this manuscript, study conception and design. The first draft of the manuscript was written by Ch. Pravallika under the guidance of Dr. K. Swapna and all authors Ib Singh Deo, M. Venkateswarulu, Sk. Mahamuda, A. S. Rao, Vijaya Prakash. G, are worked for the Resources, Writing-Editing-Review of the manuscript. All authors read and approved the final manuscript.

Data Availability Not Applicable.

Declarations

Competing Interests The authors declare no competing interests.

Ethics Approval Not applicable.

Consent to Participate Not applicable.

Consent for Publication Not applicable.

Conflicts of Interest The authors have no conflict of interest in this research.

References

1. Tanabe S (1999) Optical transitions of rare earth ions for amplifiers: how the local structure works in glass. J Non Cryst Solids 259:1–9. https://doi.org/10.1016/S0022-3093(99)00490-1

2. Himamaheswara Rao V, Syam Prasad P, Mohan Babu M, Venkateswara Rao P, Satyanarayana T, Luís F, Veeraiah N (2018) Spectroscopic studies of Dy^{3+} ion doped tellurite glasses for solid state lasers and white LEDs. Spectrochim Acta A Mol Biomol Spectrosc 188:516–524. https://doi.org/10.1016/J.SAA.2017.07.013.

3. Reddy KS, Swapna K, Mahamuda SK, Venkateswarlu M, Rao AS, Prakash GV (2018) Investigation on structural and luminescence features of Dy^{3+} ions doped alkaline-earth boro tellurite glasses for optoelectronic devices. Opt Mater (Amst) 85:200–210. https://doi.org/10.1016/J.OPTMAT.2018.08.057.

4. Deopa N, Rao AS (2017) Spectroscopic studies of Sm^{3+} ions activated lithium lead alumino borate glasses for visible luminescent device applications. Opt Mater (Amst) 72:31–39. https://doi.org/10.1016/J.OPTMAT.2017.04.067

5. Lodi TA, Dantas NF, Gonçalves TS, de Camargo ASS, Pedrochi F, Steimacher A (2019) Dy^{3+} doped calcium boroaluminate glasses and Blue Led for smart white light generation. J Lumin 207:378–385. https://doi.org/10.1016/J.JLUMIN.2018.11.045

6. Rajesh D, Ratnakaram YC, Seshadri M, Balakrishna A, Krishna TS (2012) Structural and luminescence properties of Dy^{3+} ion in strontium lithium bismuth borate glasses. J Lumin 132:841–849. https://doi.org/10.1016/j.jlumin.2011.08.050.

7. Rashad M, Ali AM, Sayyed MI, Somaily HH, Algarni H, Rammah YS (2020) Radiation attenuation and optical features of lithium borate glasses containing barium: B_2O_3.Li_2O. BaO. Ceram Int 46:21000–21007. https://doi.org/10.1016/J.CERAMINT.2020.05.165.

8. Chanthima N, Kaewkhao J, Limkitjaroenporn P, Tuscharoen S, Kothan S, Tungjai M, Kaewjaeng S, Sarachai S, Limsuwan P (2017) Development of BaO–ZnO–B_2O_3 glasses as a radiation shielding material. Radiat Phys Chem 137:72–77. https://doi.org/10.1016/J.RADPHYSCHEM.2016.03.015

9. Bagheri R, Moghaddam AK, Yousefnia H (2017) Gamma ray shielding study of barium–bismuth–borosilicate glasses as transparent shielding materials using MCNP-4C Code, XCOM program, and available experimental data. Nucl Eng Technol 49:216–223. https://doi.org/10.1016/J.NET.2016.08.013.

10. Mahmoud KA, El-Agawany FI, Tashlykov OL, Ahmed EM, Rammah YS (2021) The influence of BaO on the mechanical and gamma / fast neutron shielding properties of lead phosphate glasses, Nuclear. Eng Technol 53:3816–3823. https://doi.org/10.1016/J.NET.2021.06.005

11. Sayyed MI (2017) half value layer, mean free path and exposure buildup factor for tellurite glasses with different oxide compositions. J Alloys Compd 695:3191–3197. https://doi.org/10.1016/J.JALLCOM.2016.11.318

12. Saleem SA, Jamalaiah BC, Jayasimhadri M, Rao AS, Jang K, Moorthy LR (2011) Luminescent studies of Dy^{3+} ion in alkali lead tellurofluoroborate glasses. J Quant Spectrosc Radiat Transf 112:78–84. https://doi.org/10.1016/J.JQSRT.2010.08.017.

13. Swapna K, Mahamuda S, Rao AS, Jayasimhadri M, Sasikala T, Moorthy LR (2013) Optical absorption and luminescence characteristics of Dy^{3+} doped Zinc Alumino Bismuth Borate glasses for lasing materials and white LEDs. J Lumin 139:119–124. https://doi.org/10.1016/J.JLUMIN.2013.02.035.

14. Mahamuda S, Swapna K, Packiyaraj P, Rao AS, Prakash GV (2014) Lasing potentialities and white light generation capabilities of Dy^{3+} doped oxy-fluoroborate glasses. J Lumin 153:382–392. https://doi.org/10.1016/J.JLUMIN.2014.03.009.

15. Toufik SM, Soltani MT, Djouama T, Boutarfaia A, Poulain M (2009) New heavy metal oxide glasses based on Sb_2O_3 New heavy metal oxide glasses based on Sb_2O_3. J Optoelectron Adv Mater Symp 1:339–342

16. Deopa N, Rao AS (2018) Spectroscopic studies of single near ultraviolet pumped Tb^{3+} doped Lithium Lead Alumino Borate glasses for green lasers and tricolour w-LEDs. J Lumin 194:56–63. https://doi.org/10.1016/J.JLUMIN.2017.09.057

17. Scholze H (2012) Glass: nature, structure, and properties. https://books.google.com/books?hl=en&lr=&id=aNTcBwAAQBAJ&oi=fnd&pg=PR5&ots=Z2rVtkxSIf&sig=fG5VF4R3LQhYr0lypHbXZTi1OWQ

18. Liu R, Chen M, Zhu X, Zhou Y, Zeng F, Su Z (2020) Luminescent properties and structure of Dy^{3+} doped germanosilicate glass. J Lumin 226:117378. https://doi.org/10.1016/J.JLUMIN.2020.117378

19. Kesavulu CR, Jayasankar CK (2011) White light emission in Dy^{3+}-doped lead fluorophosphate glasses. Mater Chem Phys 130:1078–1085. https://doi.org/10.1016/J.MATCHEMPHYS.2011.08.037

20. Şakar E, Özpolat ÖF, Alım B, Sayyed MI, Kurudirek M (2020) Phy-X / PSD: Development of a user-friendly online software for calculation of parameters relevant to radiation shielding and dosimetry. Radiat Phys Chem 166:108496. https://doi.org/10.1016/J.RADPHYSCHEM.2019.108496

21. Dahiya MS, Khasa S, Agarwal A (2015) Optical absorption and heating rate dependent glass transition in vanadyl doped calcium oxy-chloride borate glasses. J Mol Struct 1086:172–178. https://doi.org/10.1016/J.MOLSTRUC.2015.01.023

22. Gautam C, Yadav AK, Singh AK (2012) A Review on Infrared Spectroscopy of Borate Glasses with Effects of Different Additives. ISRN Ceram 2012:1–17. https://doi.org/10.5402/2012/428497

23. Moustafa ES, Saddeek YB, Shaaban ER (2008) Structural and optical properties of lithium borobismuthate glasses. J Phys Chem Solids 69:2281–2287. https://doi.org/10.1016/J.JPCS.2008.04.020

24. Garrett DE (1998) Uses of Borates, Borates. 401–429. https://doi.org/10.1016/B978-012276060-0/50010-3.

25. Doweidar H, Saddeek YB (2009) FTIR and ultrasonic investigations on modified bismuth borate glasses. J Non Cryst Solids 355:348–354. https://doi.org/10.1016/J.JNONCRYSOL.2008.12.008

26. Ahamed SZ, Reddy CM, Raju BD (2013) Structural, thermal and optical investigations of Dy^{3+} ions doped lead containing lithium fluoroborate glasses for simulation of white light. Opt Mater (Amst) 35:1385–1394. https://doi.org/10.1016/J.OPTMAT.2013.02.006.

27. Carnall WT, Fields PR, Rajnak K (2003) Electronic Energy Levels in the Trivalent Lanthanide Aquo Ions. I. Pr^{3+}, Nd^{3+}, Pm^{3+}, Sm^{3+}, Dy^{3+}, Ho^{3+}, Er^{3+}, and Tm^{3+}. J Chem Phys 49:4424. https://doi.org/10.1063/1.1669893.

28. Jørgensen CK, Judd BR (2006) Hypersensitive pseudo quadrupole transitions in lanthanides 8:281–290. https://doi.org/10.1080/00268976400100321

29. Maheshvaran K, Marimuthu K (2011) Structural and optical investigations on Dy^{3+} doped boro tellurite glasses. J Alloys compd 509:7427–7433. https://doi.org/10.1016/J.JALLCOM.2011.04.055

30. Mariyappan M, Arunkumar S, Marimuthu K (2017) White light emission and spectroscopic properties of Dy^{3+} ions doped bismuth sodium fluoroborate glasses for photonic applications. J Alloys Compd 723:100–114. https://doi.org/10.1016/J.JALLCOM.2017.06.244

31. Mott NF, Davis EA (2012) Electronic processes in non-crystalline materials. https://books.google.co.in/books?hl=en&lr=&id=Pl1b_yhKHYC&oi=fnd&pg=PP1&dq=N.F.+Mott,+E.A.+Davis,+Electronic+processes+in+NonCrystalline+Materials,+Second+ed.,+Clarendon+Press,+Oxford,+1979&ots=d7yZhGG4Xe&sig=SjdScfy6fPkFUTVg_NnGrDQTMDQ.

32. Judd BR (1962) Optical Absorption Intensities of Rare-Earth Ions. Phys Rev 127:750. https://doi.org/10.1103/PhysRev.127.750

33. Opelt GS (2004) Intensities of Crystal Spectra of Rare-Earth Ions. J Chem Phys 37:511. https://doi.org/10.1063/1.1701366

34. Jørgensen CK, Reisfeld R (1983) Judd-Ofelt parameters and chemical bonding. J Less Common Met 93:107–112. https://doi.org/10.1016/0022-5088(83)90454-X

35. Khan I, Rooh G, Rajaramakrishna R, Srisittipokakun N, Wongdeeying C, Kiwsakunkran N, Wantana N, Kim HJ, Kaewkhao J, Tuscharoen S (2019) Photoluminescence and white light generation of Dy_2O_3 doped Li_2O-BaO-Gd_2O_3- SiO_2 for white light LED. J Alloys Compd 774:244–254. https://doi.org/10.1016/j.jallcom.2018.09.156

36. Klimesz B, Dominiak-Dzik G, Żelechower M, Ryba-Romanowski W (2008) Optical study of GeO_2–PbO–PbF_2 oxyfluoride glass single doped with lanthanide ions. Opt Mater (Amst) 30:1587–1594. https://doi.org/10.1016/j.optmat.2007.09.011

37. Satyanarayana T, Veeraiah N (2018) Spectroscopic studies of Dy^{3+} ion doped tellurite glasses for solid state lasers and white LEDs. Spectrochim Acta A Mol Biomol Spectrosc 188:516–524. https://doi.org/10.1016/j.saa.2017.07.013.

38. Uma V, Maheshvaran K, Marimuthu K, Muralidharan G (2016) Structural and optical investigations on Dy^{3+} doped lithium tellurofluoroborate glasses for white light applications. J Lumin 176:15–24. https://doi.org/10.1016/j.jlumin.2016.03.016

39. Vijayakumar M, Marimuthu K (2015) Structural and luminescence properties of Dy^{3+} doped oxyfluoro-borophosphate glasses for lasing materials and white LEDs. J Alloys Compd 629:230–241. https://doi.org/10.1016/J.JALLCOM.2014.12.214.

40. Vijayakumar R, Venkataiah G, Marimuthu K (2015) Structural and luminescence studies on Dy^{3+} doped boro-phosphate glasses for white LED's and laser applications. J Alloys Compd 652:234–243. https://doi.org/10.1016/J.JALLCOM.2015.08.219

41. Suresh Kumar J, Pavani K, Mohan Babu A et al (2010) Fluorescence characteristics of Dy3+ ions in calcium fluoroborate glasses. J Lumin 130:1916–1923. https://doi.org/10.1016/j.jlumin.2010.05.006

42. Ravi O, Reddy CM, Reddy BS, Deva Prasad Raju B (2014) Judd-Ofelt analysis and spectral properties of Dy3+ ions doped niobium containing tellurium calcium zinc borate glasses. Opt Commun 312:263–268. https://doi.org/10.1016/j.optcom.2013.09.044

43. Praveena R, Vijaya R, Jayasankar CK (2008) Photoluminescence and energy transfer studies of Dy^{3+}-doped fluorophosphate glasses. Spectrochim Acta A Mol Biomol Spectrosc 70:577–586. https://doi.org/10.1016/J.SAA.2007.08.001

44. Krishnaiah KV, Kumar KU, Jayasankar CK (2013) Spectroscopic properties of Dy^{3+}-doped oxyfluoride glasses for white

light emitting diodes. Mater Express 3:61–70. https://doi.org/10.1166/MEX.2013.1094

45. Karunakaran RT, Marimuthu K, Surendra Babu S, Arumugam S (2010) Dysprosium doped alkali fluoroborate glasses—Thermal, structural and optical investigations. J Lumin 130:1067–1072. https://doi.org/10.1016/J.JLUMIN.2010.01.026.

46. Chandrappa V, Basavapoornima C, Venkatramu V, Depuru SR, Kaewkhao J, Pecharapa W, Jayasankar CK (2022) A critical review and future prospects of Dy^{3+}-doped glasses for white light emission applications. Optik (Stuttg) 266:169583. https://doi.org/10.1016/J.IJLEO.2022.169583

47. Annapoorani K, Karthikeyan P, Basavapoornima Ch, Marimuthu K (2017) Investigations on the optical properties of Dy^{3+} ions doped potassium aluminium telluroborate glasses for white light applications. J Non-Cryst Solids 476:128–136. https://doi.org/10.1016/j.jnoncrysol.2017.09.038

48. Venkataiah G, Jayasankar CK (2015) Dy^{3+}-doped tellurite-based tungsten-zirconium glasses: Spectroscopic study. J Mol Struct 1084:182–189. https://doi.org/10.1016/j.molstruc.2014.11.062

49. Karthikeyan P, Arunkumar S, Annapoorani K, Marimuthu K (2018) Investigations on the spectroscopic properties of Dy^{3+} ions doped Zinc calcium tellurofluoroborate glasses. Spectrochim Acta A Mol Biomol Spectrosc 193:422–431. https://doi.org/10.1016/j.saa.2017.12.049

50. Ye Y, Wang S, An H (2019) White-light emission and chromaticity characterization of Dy3+ doped fluoride glass for standard white light source. J Non-Cryst Solids 526:119697. https://doi.org/10.1016/j.jnoncrysol.2019.119697

51. McCamy CS (1992) Correlated color temperature as an explicit function of chromaticity coordinates. Color Res Appl 17:142–144. https://doi.org/10.1002/COL.5080170211

52. Jackson DF, Hawkes DJ (1981) X-ray attenuation coefficients of elements and mixtures. Phys Rep 70:169–233. https://doi.org/10.1016/0370-1573(81)90014-4

53. Sayyed MI (2016) Bismuth modified shielding properties of zinc boro-tellurite glasses. J Alloys Compd 688:111–117. https://doi.org/10.1016/J.JALLCOM.2016.07.153

54. Tekin HO, Altunsoy EE, Kavaz E, Sayyed MI, Agar O, Kamislioglu M (2019) Photon and neutron shielding performance of boron phosphate glasses for diagnostic radiology facilities. Results Phys 12:1457–1464. https://doi.org/10.1016/J.RINP.2019.01.060

55. Perişanoğlu U, Demir L (2015) A study of K shell X-ray intensity ratios of NixCr1−x alloys in external magnetic field and determination of effective atomic numbers of these alloys. Radiat Phys Chem 110:119–125. https://doi.org/10.1016/J.RADPHYSCHEM.2015.01.032

56. Singh K, Singh H, Sharma G, Gerward L, Khanna A, Kumar R, Nathuram R, Sahota HS (2005) Gamma-ray shielding properties of CaO–SrO–B_2O_3 glasses. Radiat Phys Chem 72:225–228. https://doi.org/10.1016/J.RADPYHSCHEM.2003.11.010

57. Harima Y, Sakamoto Y, Tanaka S, Kawai M (2017) Validity of the geometric-progression formula in approximating gamma-ray buildup factors. 24–35. https://doi.org/10.13182/NSE86-A17113.

58. Bashter II (1997) Calculation of radiation attenuation coefficients for shielding concretes. Ann Nucl Energy 24:1389–1401. https://doi.org/10.1016/S0306-4549(97)00003-0

59. Sayyed MI, Elmahroug Y, Elbashir BO, Issa SAM (2017) Gamma-ray shielding properties of zinc oxide soda lime silica glasses. J Mater Sci: Mater Electron 28:4064–4074. https://doi.org/10.1007/S10854-016-6022-Z/TABLES/8